International Journal of Biological Macromolecules 387 (2027) 155194

Contents lists available at ScienceDirect

International Journal of Biological Macromolecules

journal homepage: www.elsevier.com/locate/ijbiomac

Hyaluronic acid-engineered NLCs as a macromolecular delivery platform for APOBEC3B siRNA and gemcitabine in triple-negative breast cancer: *In vitro* to *in ovo* assay

Sheikh Shahnawaz Quadir [a,b], Lauren Tonge [a], Kehinde Ross [a], Rasha Swadi [a], Garima Joshi [b,*], Imran Saleem [a,**]

[a] School of Pharmacy and Biomolecular Science, Liverpool John Moores University, Liverpool, United Kingdom
[b] Department of Pharmaceutical Sciences, Mohanlal Sukhadia University, Udaipur, Rajasthan, India

ARTICLE INFO

Keywords:
APOBEC3B siRNA
Gemcitabine hydrochloride
Breast cancer
Nanostructured lipid carriers
Hyaluronic acid
Chorioallantoic membrane (CAM) assay

ABSTRACT

Triple-negative breast cancer (TNBC) lacks targetable receptors and has poor clinical outcomes. This study combines hyaluronic acid (HA), a CD44-binding glycosaminoglycan, with APOBEC3B siRNA to engineer HA-functionalised nanostructured lipid carriers (HA-NLCs) that co-deliver gemcitabine hydrochloride (Gem HCl) and APOBEC3B siRNA to MDA-MB-231 TNBC cells. Of the four ON-TARGET plus APOBEC3B siRNA duplexes, siRNA-C gave the highest silencing (97.7% mRNA knockdown) and was selected for encapsulation. NLC entrapment (EE 68.29%) preserved its activity (97.0% suppression). The Box-Behnken-optimised Gem HCl: siRNA-NLCs measured 188.2 nm (PDI 0.284, ZP -3.30 mV). HA coating at a 3:1 NLC: HA ratio produced stable HA-NLCs (278 nm, PDI 0.137, ZP -35.3 mV), confirming successful surface functionalization and colloidal stability. Gem HCl: APOBEC3B siRNA-NLC showed the strongest cytotoxicity, enhanced apoptosis and G2.M arrest. HA-Gem HCl: APOBEC3B siRNA-NLCs showed sustained, progressive apoptotic activity, attributed to combined drug-gene therapy and HA-mediated CD44 receptor internalisation. In the chick chorioallantoic membrane (CAM) tumour model, H&E staining revealed treatment-associated histological changes, including areas consistent with necrosis, reduced tumour cellularity and altered tissue architecture. These preliminary findings warrant further quantitative validation. Overall, these findings highlight the potential of HA-coated NLCs as a platform for co-delivering gemcitabine and APOBEC3B siRNA in TNBC, warranting further mechanistic and therapeutic evaluation.

1. Introduction

Triple-negative breast cancer (TNBC) is one of the most aggressive breast cancer subtypes, accounting for approximately 10–20% of breast cancer and characterised by the absence of estrogen receptor, progesterone receptor, and HER2 expression. Owing to its highly invasive phenotype, frequent metastasis, rapid recurrence, and intrinsic resistance to conventional therapies, TNBC remains associated with poor clinical outcomes and limited treatment options despite recent advances in chemotherapy and immunotherapy [1–5].

Several small-interfering RNA (siRNA) therapeutics have now been approved for silencing of target genes in the liver, improving patient outcomes for a range of metabolic disorders [6]. Mechanistically, siRNA exploits the Argonaute-dependent RNA interference (RNAi) pathway, wherein a short double-stranded RNA molecule loaded into the RNA-induced silencing complex (RISC) drives selective recognition and degradation of target mRNA transcripts [7] However, exploiting siRNA for cancer therapy is constrained by challenges associated with delivery and efficacy against the backdrop of the complex tumour microenvironment [8]. Nonetheless, efforts have been made to develop nanoparticle systems for siRNA delivery in breast cancer, as reviewed recently [9–11].

The APOBEC3 (A3) superfamily comprises seven cytidine deaminase members (A3A-A3H), yet their oncogenic relevance in breast cancer differs markedly. A3C, A3D, A3F, and A3G are predominantly cytoplasmic with absent or inconsistent breast cancer expression, whilst

* Correspondence to: G. Joshi, Department of Pharmaceutical Sciences, Mohanlal Sukhadia University, Udaipur, India.
** Corresponding author.
E-mail addresses: drgarimajoshi@mlsu.ac.in (G. Joshi), I.Saleem@ljmu.ac.uk (I. Saleem).

https://doi.org/10.1016/j.ijbiomac.2026.155194
Received 5 August 2026; Received in revised form 30 October 2026; Accepted 5 November 2026
Available online 9 November 2026
0141-8130/© 2026 The Authors. Published by Elsevier B.V. This is an open access article under the CC BY license (http://creativecommons.org/licenses/by/4.0/).

endogenous A3A nuclear activity is largely undetectable in breast cancer cell lines under basal conditions [12]. APOBEC3B (A3B), by contrast, is uniquely characterised by constitutive nuclear localisation, mediated through a functional NLS in its N-terminal zinc-coordinating domain, conferring direct and sustained access to replicating genomic DNA, a structural advantage absent in all other family members [13,14].

Burns et al. established A3B as the sole APOBEC3B member consistently upregulated ≥3-fold across breast cancer cell lines and overexpressed in 50% of primary breast tumours, with A3A expression largely undetectable at endogenous levels [15], whilst its constitutive nuclear deaminase activity generates the characteristic SBS2 and SBS13 COSMIC mutational signatures, driving TP53 inactivation, intratumour heterogeneity, and clonal evolution [16,17].

Clinically, Law et al. demonstrated that A3B promotes tamoxifen resistance in ER-positive breast cancer [18] and Razavi et al. confirmed A3B-driven mutations confer broad multi-drug resistance through accumulation of APOBEC-class alterations in resistance-associated genes [19]. A3B is constitutively expressed in the MDA-MB-231 TNBC model employed here, whilst A3A activity remains negligible [15,20]. Burns et al. identified A3B as non-essential in normal tissues, offering a favourable therapeutic window not shared by other family members [15]. These converging lines of evidence, constitutive nuclear localisation, breast cancer-specific overexpression, mechanistic role in genomic instability and therapeutic resistance, and a safe normal tissue profile uniquely distinguish A3B and provide a robust rationale for its selection as the siRNA target in this study.

Increasing evidence identifies APOBEC3B as a key driver of genomic instability, tumour evolution, and therapeutic resistance in breast cancer. Persistent overexpression of APOBEC3B promotes cytidine deamination-induced mutagenesis, generating the characteristic APOBEC mutational signatures that contribute to intra-tumoural heterogeneity and disease progression. Consequently, selective silencing of APOBEC3B using small interfering RNA (siRNA) has emerged as a promising strategy to suppress tumour evolution and enhance therapeutic sensitivity [17,21,22].

Combining gene silencing with chemotherapy offers an attractive approach for overcoming drug resistance in TNBC. Gemcitabine hydrochloride (Gem HCl) is a nucleoside analogue widely used in advanced breast cancer; it inhibits DNA synthesis and induces apoptosis in rapidly proliferating tumour cells. Simultaneous delivery of Gem HCl and APOBEC3B siRNA is therefore expected to provide a complementary therapeutic effect by directly inducing tumour cell death while suppressing mutation-driven resistance mechanisms. However, the clinical translation of this combination remains challenging because Gem HCl exhibits rapid systemic clearance and poor bioavailability. In contrast, siRNA is susceptible to limited cellular uptake and inefficient intracellular delivery [23]. Previous studies have highlighted the therapeutic potential of co-delivering Gem HCl and siRNA-mediated gene silencing agents, including anti-NF-kB (Norouzi et al.), HIF-1α siRNA (Zhao et al.), and SERPINB9 siRNA (Huang et al.), to overcome tumour progression and chemoresistance [24–26].

Nanostructured lipid carriers (NLCs) have emerged as promising co-delivery vehicles capable of simultaneously encapsulating chemotherapeutic agents and nucleic acids while protecting them from premature degradation and enhancing intracellular delivery. Furthermore, surface functionalization with hyaluronic acid (HA) enables active targeting of CD44-overexpressing TNBC cells through receptor-mediated endocytosis, thereby improving tumour-selective uptake and reducing off-target toxicity. Previous studies have demonstrated the feasibility of NLC-mediated co-delivery of chemotherapeutics and siRNA [1,5,27–29] However, targeted co-delivery of Gem HCl and APOBEC3B siRNA *via* CD44-targeted hyaluronic acid-coated NLCs for TNBC has not been systematically investigated before.

Therefore, the present study aimed to develop hyaluronic acid-coated NLCs co-loaded with Gem HCl and APOBEC3B siRNA for targeted treatment of CD44-overexpressing MDA-MB-231 triple-negative breast cancer cells. The proposed nanoplatform was designed to enhance tumour-specific delivery, improve intracellular gene silencing, and achieve enhanced combinatorial anticancer activity by simultaneously inhibiting DNA synthesis and suppressing APOBEC3B mediated genomic instability and drug resistance.

2. Materials

Gemcitabine Hydrochloride was purchased from Merck (Sigma-Aldrich). APOBEC3B siRNA was purchased from Dharmacon, UK. APOBEC3B and GAPDH forward and reverse primers were purchased from Sigma-Aldrich. Gattefosse, UK, kindly supplied glycerol monostearate; Labrasol and phosphatidylcholine; and Tween 80 were purchased from Himedia. Hyaluronic Acid Sodium Salt (M.W. 200–400 kDa) were purchased from Glentham Life Science. Annexin V Apoptosis Detection Kit, RNase A and Lipofectamine were purchased from Thermofischers. Rhodamine-B and 4,6-diamidino-2-phenylindole (DAPI) were purchased from Himedia. The cell line studies were performed on MDA-MB-231 cells, which were purchased from the UK Health Security Agency (ECCA catalogue no: 92020424). MDA-MB-231 cells were cultured in streptomycin (100 mg/mL) with high-glucose DMEM medium, supplemented with 10% FBS and penicillin 100 U/mL, in a humidified atmosphere containing 5% CO_2 at 37 °C. Finally, the cells were sub-cultured to achieve 80–90% growth for further experiments. All other chemicals and reagents used were of analytical or chromatographic grade.

3. Methods

3.1. Optimisation of APOBEC3B siRNA by gene expression analysis using real-time quantitative PCR (RT-qPCR)

To investigate the role of APOBEC3B in breast cancer pathogenesis, an siRNA-mediated gene knockdown optimisation study was conducted in MDA-MB-231 cells. For siRNA optimisation, four individual ON-TARGET plus siRNA duplexes (Dharmacon/Horizon Discovery) targeting distinct regions of the APOBEC3B transcript, designated siRNA-A (5′-CACAUGGGCUUUCUAUGCA-3′), siRNA-B (5′-CCUGAUGGAUCCAGACACA-3′), siRNA-C (5′-UGACCUACGAUGAGUUUGA-3′) and siRNA-D (5′-GUGAUUAAUUGGCUCCAUA-3′) were independently assessed alongside a non-targeting siRNA negative control and a mock (untransfected). For transfection, cells were seeded at a density of 1.5×10^5 cells/well into 6-well plates in complete growth medium and allowed to adhere for 24 h. Total RNA was extracted from all groups 24 h post-transfection under strictly RNase-free conditions using the ReliaPrep™ RNA Miniprep System (Promega, USA), yielding A260/A280 ratios of 1.8–2.0 and A260/A230 ratios of 2.0–2.2. Complementary DNA (cDNA) was synthesised from 400 ng of total RNA per reaction using the High-Capacity cDNA Reverse Transcription Kit (Applied Biosystems), under the sequential thermal conditions. APOBEC3B mRNA expression levels were subsequently quantified by SYBR Green-based quantitative real-time PCR (RT-qPCR) on a Rotor Gene Q system (QIAGEN), using gene-specific primers for APOBEC3B (forward: 5′-CGCCAGACCTACTTGTGCTA-3′; reverse: 5′-GCCACAGAGAAGATTCTTAGCC-3′) and the endogenous reference gene GAPDH (forward: 5′-CAAGGTCATCCATGACAACTTTG-3′; reverse: 5′-GTCCACCACCCTGTTGCTGTAG-3′). The primer sequence for APOBEC3B was adopted from a previously published study [28]. The qRT-PCR was performed with an initial denaturation of 95 °C for 5 min, followed by 40 cycles of 95 °C for 30 s, 64 °C for 40 s, and 72 °C for 40 s. Relative APOBEC3B miRNA expression was determined by the $2^{-\Delta\Delta Cq}$ method using GAPDH as the endogenous reference and the mock group as calibrator per MIQE guidelines [30]. Knockdown efficiency of each siRNA duplex was expressed as the percentage reduction in APOBEC3B transcript levels relative to the untreated control.

3.2. Formulation of Gem HCl: APOBEC3B siRNA-loaded NLCs

3.2.1. Screening of lipids and surfactants

The solubility study was performed to obtain the most suitable candidate for a nanostructured lipid carrier formulation with high drug loading capacity. Solubility studies were performed in surfactants (Tween 20, Tween 40 and Tween 80) and co-surfactants (Methanol and Ethanol). Solubility of Gem HCl in lipids was performed in solid lipids (Precirol® ATO 5, Compritol® 888 ATO and Glycerol Monostearate) and liquid lipids (LL) (Labrasol and Labrafil). An excess of Gem HCL was allowed to dissolve in 2 mL of water for the aqueous phase, and 500 mg of each solvent was added to the lipids on a thermostat-controlled shaker bath for 24 h at 72^0C to achieve dissolution equilibrium. Lastly, the sample was centrifuged at 10,000 rpm for 10 min, and the supernatant was dissolved in a water: chloroform (1:1) ratio, and dilution was assessed under a UV–visible spectrophotometer. All the studies were conducted in triplicate.

3.2.2. Formulation of APOBEC3B siRNA-loaded NLCs

APOBEC3B siRNA was loaded within NLCs using the hot micro-emulsification technique. 2% of the total lipid was utilised with a mass ratio of 4:3:3 for solid lipid: liquid lipid: phosphatidylcholine. Firstly, solid lipid (GMS) and liquid lipid (Labrasol) were allowed to melt at 70 °C. APOBEC3B siRNA was allowed to dissolve in 1 mL of water (as an internal aqueous phase) in a separate beaker. Lastly, phosphatidylcholine was allowed to dissolve in a portion of ethanol containing Tween 80 before adding it to the lipid phase to obtain a clear microemulsion. A clear microemulsion was added dropwise using a prewarmed syringe in the remaining portion of water (approx. 90%), before being cooled at 4 °C and stirred continuously for 30 min at 3000 rpm using a T25 digital

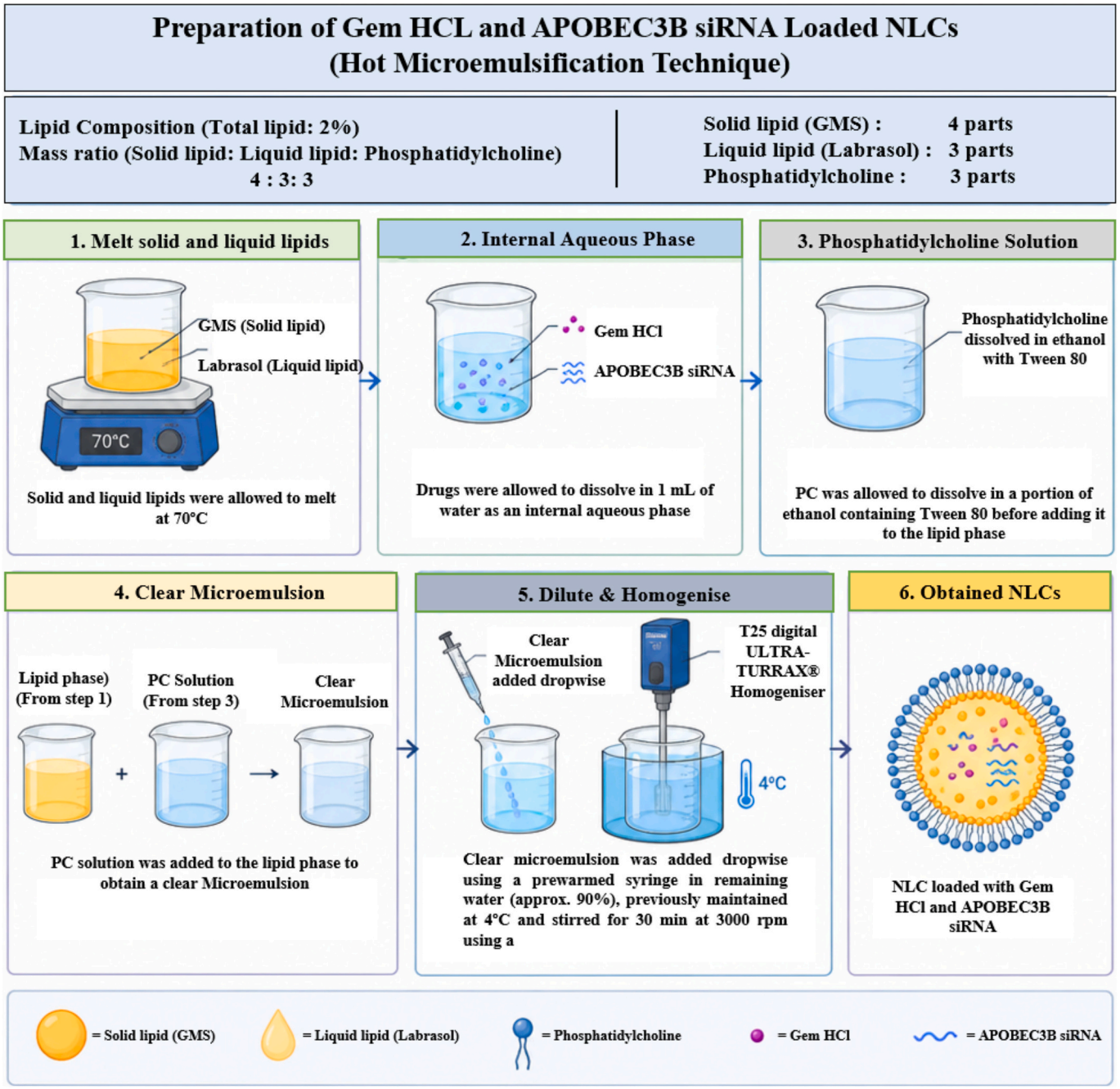

Fig. 1. A scheme for the preparation of Gem HCl and APOBEC3B siRNA loaded NLCs using a T25 digital ULTRA-TURRAX® homogeniser.

ULTRA-TURRAX® homogeniser to obtain NLCs [29].

3.2.3. Transfection of APOBEC3B siRNA-loaded NLCs on MDA-MB-231 cells

Transfection studies of APOBEC3B siRNA-loaded NLCs were performed as described earlier in the optimisation section. Instead of naked siRNA, APOBEC3B siRNA-loaded NLCs were used to understand their effect on gene expression. Similarly, RNA extraction, RNA quantification, cDNA synthesis and qPCR analysis using the motor gene were performed as discussed in the optimisation section.

3.2.4. Formulation of Gem HCl: APOBEC3B siRNA-loaded NLCs

Gem HCl (10 mg) and APOBEC3B siRNA (60 pmol) were loaded within NLCs using the hot microemulsification technique. 2% of the total lipid was utilised with a mass ratio of 4:3:3 for solid lipid: liquid lipid: phosphatidylcholine. Firstly, solid lipid (GMS) and liquid lipid (Labrasol) were allowed to melt at 70 °C. Secondly, Gem HCl and APOBEC3B siRNA were allowed to dissolve in 1 mL of water (as an internal aqueous phase) in a separate beaker. Lastly, phosphatidylcholine was allowed to dissolve in a portion of ethanol containing Tween 80 before adding it to the lipid phase to obtain a clear microemulsion. A clear microemulsion was added dropwise using a prewarmed syringe in the remaining portion of water (approx. 90%), before being cooled at 4 °C and stirred continuously for 30 min at 300 rpm using a T25 digital ULTRA-TURRAX® homogeniser to obtain NLCs. The schematic formulation steps are shown in Fig. 1.

3.2.4.1. Box–Behnken design optimisation. In the present study, drug-loaded NLCs were optimised by a 3-factor, 3-level Box-Behnken Design (BBD) technique to get the best optimised composition. The software (Design-Expert) was utilised to optimise the prepared NLCs. Three independent variables used for the experiment were GMS (X1), Labrasol (X2) and Tween 80 (X3), as shown in Table 1. The impacts of the three independent variables were identified by the dependent variables, such as entrapment efficiency (EE) in % as Y1 and particle size (PS) in nm as Y2. The design formulation gives 15 different experimental compositions with 3 centre points. The point prediction technique was performed to select the optimised drug-loaded NLCs. On the basis of maximum entrapment and minimum particle size, statistical analysis was used to assess the independent variables affecting the responses as well as the interaction between the factors.

3.2.4.2. Surface modification of Gem HCl: APOBEC3B siRNA NLCs using hyaluronic acid (HA). Hyaluronic acid (HA) was coated on nanostructured lipid carriers (NLCs) by electrostatic interaction between the positively charged surface of NLCs and the negatively charged HA. HA solutions at several concentrations, 0.05% (0.5 mg/mL), 0.10% (1 mg/mL), 0.15% (1.5 mg/mL), and 0.20% (2 mg/mL) were made in nuclease-free water for Optimisation. To determine the ideal coating conditions, various NLC: HA mass ratios were computed while keeping the NLC mass at 40 mg/mL. The chosen ratios, which represented different levels of HA in relation to the NLC mass, were 3:1, 2:1, 1:1, 1:2 and 1:3 (NLC: HA). To obtain these ratios, a predetermined amount of NLC dispersion was added dropwise to the appropriate quantities of HA solution and stirred for 30 min at 1000 rpm on a magnetic stirrer to enable homogeneous coating through electrostatic interaction [31].

Table 1
Independent and dependent variables used in BBD design for the Gem HCl: APOBEC3B siRNA-NLCs.

Factors	Actual coded factors		
Independent variables	Low (−1)	Medium (0)	High (+1)
X1 = Amount of GMS (mg)	80	160	240
X2 = Amount of Labrasol (mg)	60	120	180
X3 = Amount of Tween 80 (mg)	200	400	600
Dependent Variables	**Goal**		
Y1 = Entrapment efficiency (EE; %)	Maximum		
Y2 = Particle size (PS; nm)	Minimum		

3.3. Characterisation studies

3.3.1. Particle characterisation

The prepared Gem HCl-APOBEC3B siRNA-loaded NLCs were characterised for particle size, PDI and Zeta potential. The size of the diluted samples was measured by dynamic light scattering (Zetasizer Nano ZS90, Malvern). The zeta potential of optimised NLCs was assessed to determine the charge on the NLC surface. The surface morphology of formulated NLCs was evaluated using transmission electron microscopy. The samples were stained with phosphotungstic acid and dried on the copper grid before analysis. The sample was visualised under the microscope at high resolution, and micrographs were captured and further visualised with the help of imaging viewer software.

3.3.2. Entrapment efficiency and drug loading

Gem HCl-APOBEC3B siRNA-loaded NLCs were placed in a centrifuge tube and centrifuged for 1 h at 4 °C at 16000 RPM (Velocity 18R Pro Versatile Refrigerated Centrifuge, Dynamica). After centrifugation, the supernatant layer was separated and analysed under UV for unentrapped Gem HCl and NanoDrop for unentrapped siRNA. Similarly, the obtained down-layer chip was separated out and dissolved in chloroform: water (1:1) for complete solubilization of the drug and lipids. Furthermore, the solution was analysed by UV–Vis spectroscopy at the respective wavelength for the unentrapped and entrapped drug. For drug loading, the amount of drug entrapped per 100 parts of carrier was reported using eqs. 1 and 2.

$$\%EE = \text{Weight of drug in pellet} / \text{Weight of drug initially added in the NLCs} \times 100 \quad (1)$$

$$\%DL = \text{Weight of the drug in pellet} / \text{Weight of the recovered NLC pellets} \times 100 \quad (2)$$

3.3.3. FTIR spectroscopy

FTIR analysis was performed to evaluate the chemical compatibility and confirm the successful coating of hyaluronic acid (HA) on Gem HCl-loaded nanostructured lipid carriers (NLCs). The spectra of pure Gem HCl, hyaluronic acid, and HA-coated Gem HCl NLCs were recorded using an FTIR spectrophotometer, which was investigated by FTIR (NICOLET™ SUMMIT™-ThermoFisher Scientific). The background was scanned for 16 scans before placing a sample on the ATR disk (Attenuated Total Reflectance Accessory), which is ideal for analysing solids, liquids, pastes, or powders. Then this mixture was analysed in the IR range of 400 to 4000 cm^{-1} and compared with the drug library.

3.4. Evaluation studies

3.4.1. In vitro drug release and release kinetics

The *in vitro* release of Gem HCl-APOBEC3B siRNA-NLCs was determined using the dialysis bag diffusion technique. Drug-loaded NLCs were compared to plain drug suspension (equivalent to 1 mg of drug). The release studies were performed in PBS at pH 7.4. The dialysis bag was immersed in 50 mL of receptor phase, which was stirred at 100 rpm and maintained at 37 ± 2 °C. The receptor compartment was covered during the entire process. The aliquots of 2 mL each were withdrawn at regular time intervals (0, 2, 4, 6, 12, 24, 48, 72 h), and the medium was replenished with fresh medium to maintain sink conditions. The experiment was performed in triplicate, and the average values were taken. The data obtained were fitted into various models to find the best-fitted release models.

3.4.2. Cytotoxicity assay

Cytotoxicity of NLCs, Gem HCl-NLCs, and plain drug suspension was assessed against MDA-MB-231 cells to determine percent cytotoxicity and the dose-response curve using the MTT assay. Cells were seeded in 96-well plates at 1×10^4 cells/well. Plates were incubated at 37 °C in a humidified CO_2 (5%) incubator for 24 h. Then the cells were treated with different concentrations in the range of 5–100 μM. After 24 h of incubation, the supernatant of each well was removed, and the cells were incubated for 4 h with 100 μL of MTT reagent (1 mg/mL) in serum-free MEM. MTT was removed, and the formed insoluble formazan crystals were dissolved in 100 μL of DMSO solution, and the optical density was measured at 570 nm using a microplate reader (680-XR, Bio-Rad Laboratories, France). Untreated cells were taken as a control with 100% viability, and cells without MTT were used as a blank to calibrate the spectrophotometer to zero absorbance. The percentage viability was calculated using eq. 3.

$$\%\text{Viability} = \text{Abs of Test}/\text{Abs of Control} \times 100 \tag{3}$$

3.4.3. RNAiMAX transfection (MTT assay)

Lipofectamine™ RNAiMAX reagent and the corresponding siRNA formulations were made by independent dilution in serum-free culture medium for the transfection procedure. For each 96-well plate, 25 μL of serum-free medium was diluted with 1.5 μL of Lipofectamine RNAiMAX reagent. Simultaneously, siRNA and its equivalent formulations, such as siRNA-NLCs or specific combination treatment groups, were diluted in an equal volume of 25 μL serum-free medium in a different micro-centrifuge tube. To facilitate the spontaneous self-assembly of siRNA–lipid complexes before cellular application, the two diluted components were combined in a 1:1 volumetric ratio, gently mixed, and incubated for 5 min at room temperature.

APOBEC3B siRNA, APOBEC3B siRNA-loaded NLCs, mock (untreated control), mock NLCs, Lipofectamine control, APOBEC3B siRNA + Gem HCl, and APOBEC3B siRNA + Gem HCl-loaded NLCs were the experimental groups. After transfection, cells were cultured for 24 to 72 h at 37 °C in 5% CO_2. After incubation, the supernatant of each well was removed, and the cells were incubated for 4 h with 100 μL of MTT reagent (1 mg/mL) in serum-free MEM. MTT was removed, and the formed insoluble formazan crystals were dissolved in 100 μL of DMSO solution, and the optical density was measured at 570 nm using a microplate reader (680-XR, Bio-Rad Laboratories, France). Untreated cells were taken as a control with 100% viability, and cells without MTT were used as a blank to calibrate the spectrophotometer to zero absorbance. The percentage viability was calculated using the equation (Eq. 3).

3.4.4. Intracellular uptake study by MDA-MB-231 cells using confocal microscopy

Cells were seeded at a density of 1×10^6 cells/well on a Thermo Scientific™ Nunc™ Lab-Tek™ II Chambered Coverglass and allowed to adhere for 24 h. After 24 h, cells were washed with fresh medium and incubated with 100 μL of rhodamine B-loaded NLCs at mg/mL. To identify the time-dependent uptake, the cells were incubated with dye-loaded NLCs and plain dye solution for 1 and 2 h. The cell monolayer was fixed with cold methanol for 20 min and rinsed with PBS. After rinsing, the nuclei were stained with DAPI for 3 min and rinsed again with PBS and observed using a Carl Zeiss confocal laser microscope (LSM 710) at DAPI (Blue fluorescence): excitation wavelength = 347 nm, emission wavelength = 483 nm and Rhodamine B (red-to-orange fluorescence): excitation wavelength = 545 nm, emission wavelength = 580 nm. The images were analysed by Zen imaging software. Intracellular fluorescence intensity was quantified from confocal images using ImageJ software (NIH, USA) by calculating the corrected total cell fluorescence (CTCF) using eq. 4.

$$\text{CTCF} = \text{Integrated Density} - (\text{Area of selected cell} \times \text{Mean Fluorescence of Background}) \tag{4}$$

3.4.5. Cell migration assay

MDA-MB-231 cells were inoculated into 6-well plates (3×10^5 cells/well). When the cell confluency reached about 80–90%, a wound scratch with an equal distance was created using a 200 μL sterile pipette tip at 0 h. The cell layer was washed with prewarmed PBS to remove the debris. After 12 and 24 h of post-culture of cells with control, Plain drug and drug-loaded-NLCs. The areas of the wound scratches were calculated under a Leica DM IL LED microscope (Leica, Wetzlar, Germany) and further analysed using ImageJ software. The migration rate was determined using eq. 5 [22].

$$\text{Migration rate (\%)} = (\text{Wound area at 0 h} - \text{Wound area at t})/\text{Wound area at 0 h} \times 100 \tag{5}$$

3.4.6. In vitro apoptosis assay

Apoptosis was assessed using an Annexin V-FITC apoptosis detection kit (*E*-Bioscience™). MDA-MB-231 (3×10^4 cells per well) were treated with free Gem HCl (10 μM), Gem HCl: APOBEC3B siRNA-NLCs and HA-Gem HCl: APOBEC3B siRNA-NLCs at an equivalent drug concentration of 10 μM, and incubated at 37 °C for 24 h. Following treatment, MDA-MB-231 cells were harvested by trypsinisation, washed twice with cold PBS, and resuspended in 1× binding buffer. The cells were then stained with 5 μL of Annexin V-FITC and 5 μL of propidium iodide (PI) and incubated for 15 min at room temperature in the dark. After adding 400 μL of binding buffer, the stained cells were immediately analysed by flow cytometry (BD Accuri™ C6). The percentages of viable, early apoptotic, late apoptotic and necrotic cells were quantified, and the total apoptotic rate was calculated as the sum of early and late apoptotic cells.

3.4.7. Cell cycle distribution assay

Cell cycle distribution was assessed to elucidate the mechanism of drug-induced cell death and quantify the sub-G1 apoptotic population. MDA-MB-231 cells (3×10^4 cells per well) were treated under the above-mentioned conditions for 24 h. Post-treatment, cells were harvested by trypsinisation, washed with PBS (7.4) and fixed in 70% ethanol overnight at 4 °C. The fixed cells were subsequently washed to remove residual ethanol, treated with RNase A to eliminate RNA interference and stained with PI for 30 min at 37 °C in the dark. Cell cycle alterations were analysed using flow cytometry.

3.5. Chorioallantoic membrane (CAM) model for evaluating antitumour activity

The CAM assay was conducted across three independent biological replicates, with a total of 36 fertilised brown chicken eggs (Medeggs LTD, UK) allocated equally across three treatment groups: untreated control, free Gem HCl, and HA-Gem HCl: APOBEC3B siRNA-NLLCs at 12 eggs per group per batch. A schematic of the experimental design is depicted in Fig. 2. Eggs were incubated horizontally at 38 °C with 40% relative humidity in a Multihatch Mark II incubator (Brinsea, UK), with the commencement of incubation designated as embryonic day 0 (E0). On E3, egg surfaces were disinfected with 70% ethanol, approximately 4 mL of albumin was withdrawn *via* a 19G needle at a 45° angle to prevent embryo membrane adhesion, and a 1 × 1.5 cm window was excised from the upper eggshell surface before resealing with adhesive tape and returning eggs to the incubator. On E7, MDA-MB-231 cells harvested using 0.005% trypsin-EDTA, washed by centrifugation at 1000 rpm for 5 min and resuspended at 2×10^6 cells in 10–12 μL of fresh medium, were implanted directly onto the CAM surface following gentle membrane scarification with a 100% ethanol-dipped strip and pre-treatment with 5 μL of 0.05% trypsin to facilitate cell adhesion. Drug treatments, comprising Gem HCl 10 μM, siRNA 60 pmol, or equivalent

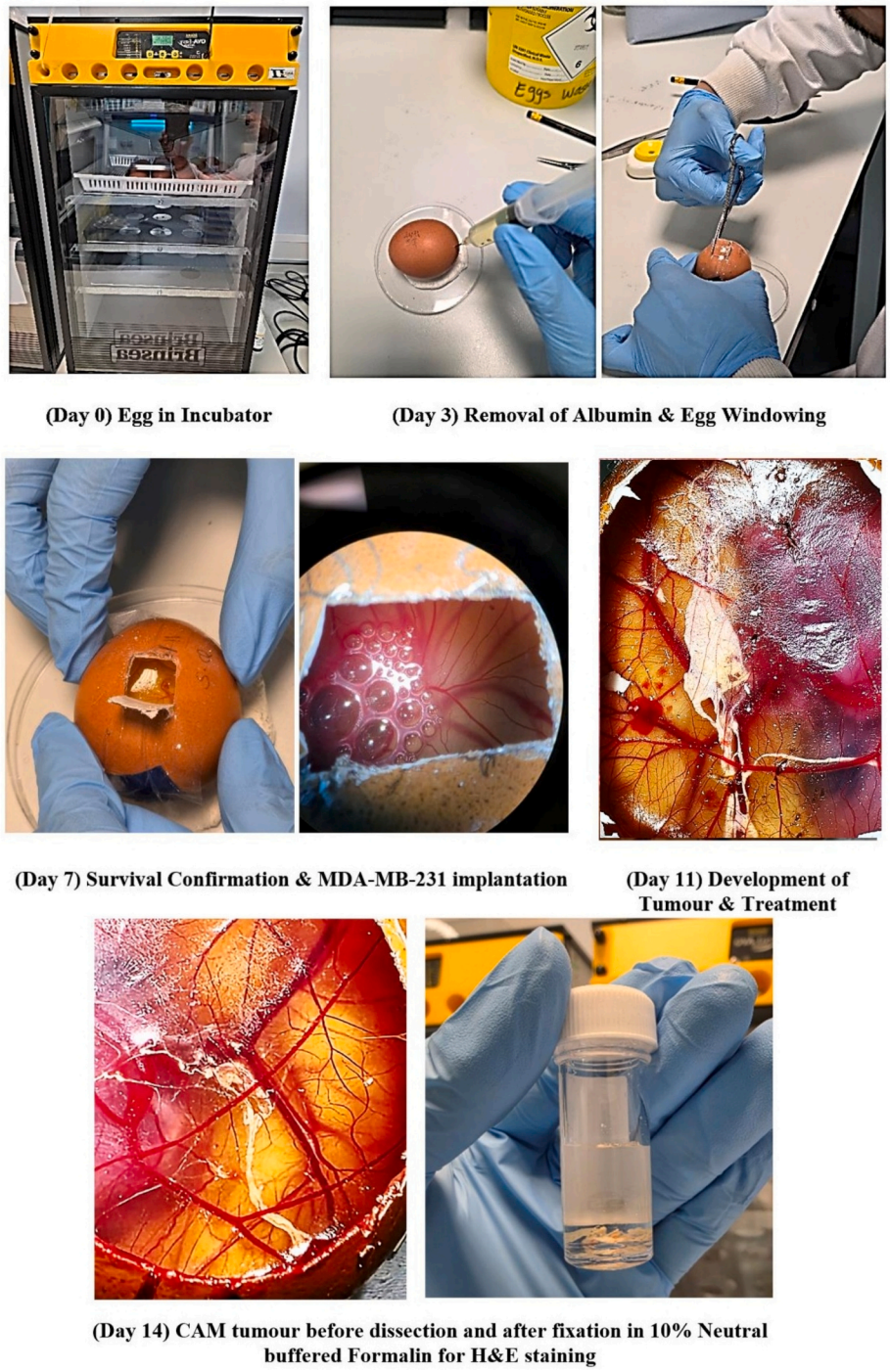

Fig. 2. Establishment of the ex-ovo chorioallantoic membrane (CAM) xenograft model for evaluation of antitumour activity. Fertilised eggs were incubated (Day 0), followed by albumin removal and egg windowing (Day 3). On Day, embryo viability was confirmed, and MDA-MB-231 cells were implanted onto the CAM. Tumour development and treatment were monitored on Day 11. On Day 14, CAM tumours were harvested and fixed in 10% neutral-buffered formalin for haematoxylin and eosin staining and histopathological evaluation. Representative images depict the key stages of the ex-ovo CAM assay.

formulations prepared in 200 μL Dulbecco's PBS (DPBS), were administered intraallantoically on E11 *via* a 23G needle, with control embryos receiving 200 μL DPBS alone; all eggs were resealed and maintained until E14. On E14, surviving embryos were examined under a Leica MI65 FC stereomicroscope; excised tumours were dissected with straight-tip forceps and scissors and immediately fixed in 10% formalin, and representative images were captured before and after resection using a Leica DFC425C camera with LAS4.0 software. Tumour area (mm2) was quantified from stereomicroscopic images using ImageJ software following scale calibration (scale bar = 2 mm at × 10 magnification) by freehand selection of the tumour nodule, and TGI% was calculated relative to the untreated control [32]. Vascular density was determined by Colour Threshold analysis of red-stained vessel pixels in ImageJ, expressed as a percentage of total image area [33]. For histological evaluation, tissue sections were stained with haematoxylin for nuclear visualisation, differentiated in 0.5% acid alcohol, blued in Scott's tap water, dehydrated through a graded alcohol series, cleared in xylene, and mounted under 22 × 50 mm coverslips using DPX mounting

medium [34].

3.6. Statistical analysis

Results were evaluated as the mean ± S. One-way ANOVA was performed to evaluate the differences between the treated group and the control group. *P*-value <0.05 was considered significant (GraphPad Prism V 10.6.1).

4. Results

4.1. Optimisation of APOBEC3B siRNA by gene expression analysis using real-time quantitative PCR (RT-qPCR)

To identify the most effective APOBEC3B-targeting siRNA duplex, MDA-MB-231 cells were transfected with four ON-TARGETplus siRNAs (A-D; Dharmacon), alongside a non-targeting negative control and a mock (untransfected) control. Total RNA extracted from all groups 24 h post-transfection yielded A260/A280 ratios of 1.8–2.0 and A260/A230 ratios of 2.0–2.2, confirming high purity and suitability for downstream

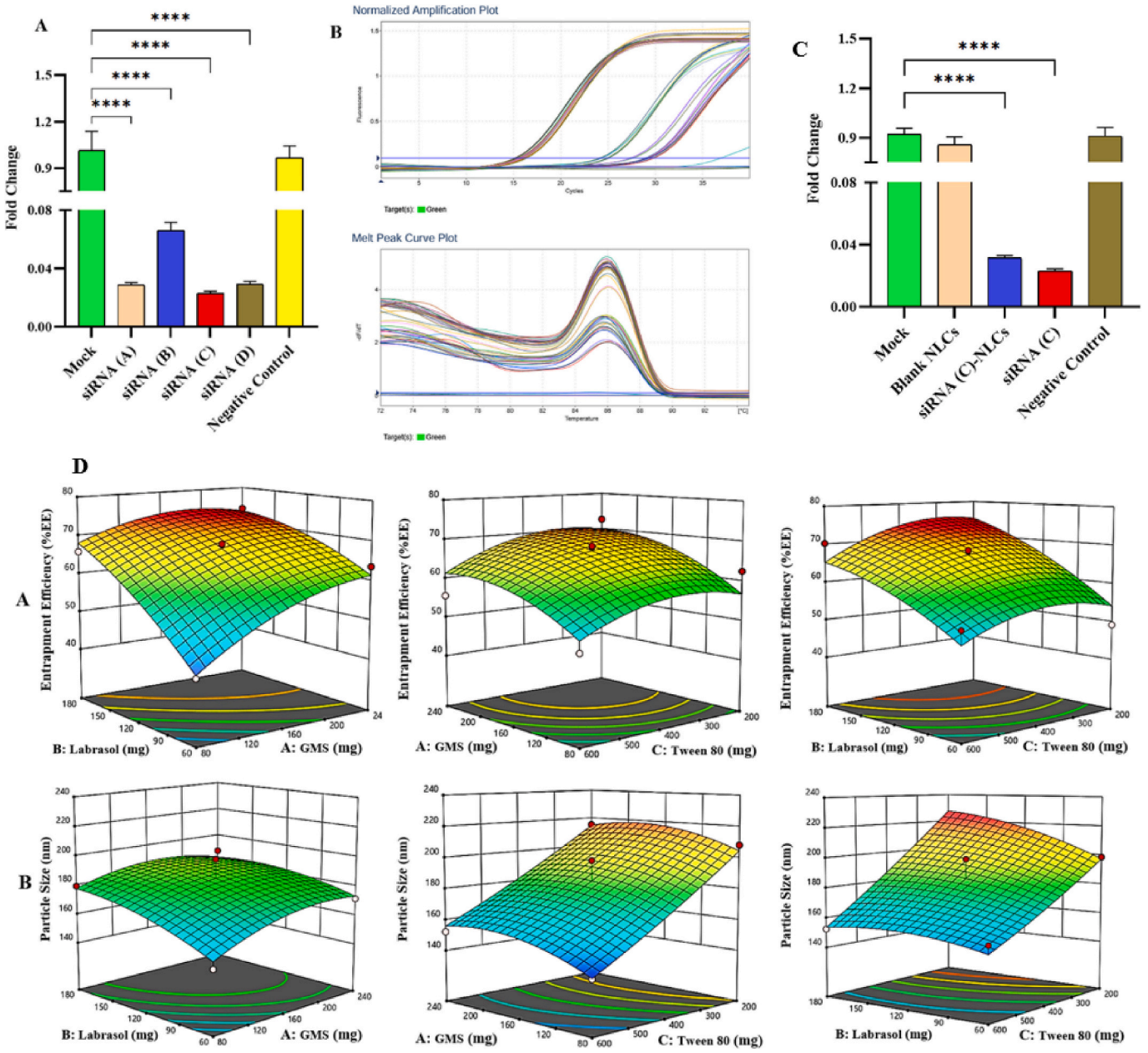

Fig. 3. (A) illustrates the gene silencing efficacy of APOBEC3B siRNA on MDA-MB-2331 cells. Statistical evaluation of relative APOBEC3B mRNA expression ($2^{-\Delta\Delta Cq}$) across all treatment groups was conducted using one-way ANOVA with Dunnett's multiple comparison test, using the mock-transfected group as the reference calibrator, **** $P < 0.0001$. (B) Validation of APOBEC3B gene expression by qRT-PCR in MDA-MB-231 cells. Normalised amplification plots depicting amplification of the APOBEC3B transcript and melt peak curve plots demonstrating specific target amplification. (C) Gene silencing efficiency of APOBEC3B siRNA (C)-loaded NLCs in MDA-MB-231 cells. Relative APOBEC3B mRNA expression was quantified by qRT-PCR using the $2^{-\Delta\Delta Cq}$ method 24 h after treatment. APOBEC3B siRNA (C)-NLCs significantly reduced gene expression compared with the mock and blank NLC groups. Data are presented as mean ± SD ($n = 3$). (D) Three-dimensional response surface plots generated using the BBD illustrating the interactive effects of GMS (A), Labrasol (B), and Tween 80 (C) on (A) entrapment efficiency (%EE) and (B) particle size (nm) of drug-loaded NLCs. The plots demonstrate the combined influence of formulation variables on the Optimisation of NLC formulation.

RT-qPCR analysis.

The mock (1.014 ± 0.214) and negative control (0.965 ± 0.136) groups showed comparable APOBEC3B expression levels, with no significant difference observed between them ($p = 0.9647$). In contrast, all APOBEC3B-targeting siRNAs significantly reduced APOBEC3B mRNA expression compared with the mock control ($p < 0.0001$). Among the tested duplexes, siRNA-C demonstrated the highest silencing efficiency, reducing APOBEC3B expression to 0.023 ± 0.003 (approximately 97.7% knockdown). siRNA-A and siRNA-D produced comparable suppression (0.029 ± 0.003 each; approximately 97.1% knockdown), whereas siRNA-B achieved a relatively lower but still substantial reduction (0.066 ± 0.010; approximately 93.4% knockdown) (Fig. 3-A).

One-way ANOVA analysis of $2^{-\Delta\Delta Cq}$ values revealed a highly significant difference among treatment groups ($F(5,12) = 67.35$, $p < 0.0001$). Subsequently, Dunnett's multiple comparison test confirmed a significant reduction in APOBEC3B expression for all siRNA-treated groups relative to the mock control ($P < 0.0001$). Amplification plots and melt curve analysis further verified successful and specific amplification of the APOBEC3B transcript, demonstrating assay reliability and specificity (Fig. 3-B).

4.2. Formulation of Gem HCl-APOBEC3 siRNA (C)-loaded NLCs

4.2.1. Screening of lipids and surfactants

The solubility of Gem HCl was systematically evaluated across lipids and surfactants to identify the optimal excipient composition for NLC preparation. Among the surfactants screened, Tween 80 demonstrated the highest solubility for Gem HCl (5.48 ± 1.46 mg/g), followed by Tween 20 (5.03 ± 2.34 mg/g) and Tween 40 (2.90 ± 1.27 mg/g); hence, Tween 80 was selected as the surfactant of choice. Regarding lipid selection, Labrasol exhibited the highest solubility among liquid lipids (5.52 ± 1.45 mg/g) compared to Labrafil (3.28 ± 2.32 mg/g), and was therefore selected as the liquid lipid. Among solid lipids, glycerol monostearate (GMS) demonstrated the highest solubility for Gem HCl (3.42 ± 1.45 mg/g), compared to Precirol® ATO 5 (3.18 ± 2.47 mg/g) and compritol®888 ATO (2.80 ± 1.36 mg/g). Collectively, GMS, Labrasol and Tween 80 were identified as the optimal compositions for preparation of Gem HCl-NLCs.

4.2.2. Formulation, characterisation and gene silencing efficiency of APOBEC3B siRNA (C)-NLCs

APOBEC3B siRNA (C)-loaded NLCs were successfully prepared using the hot microemulsification technique. Physicochemical characterisation demonstrated a mean particle size of 117.1 nm, with a PDI of 0.3, indicating a narrow and homogeneous particle size distribution. The formulation exhibited a near-neutral surface charge, with a zeta potential of −2.93 mV. Quantification of encapsulated siRNA by NanoDrop spectrophotometry at 260 nm revealed an entrapment efficiency of 68.29%, corresponding to a measured siRNA concentration of 253 ng, confirming successful incorporation of APOBEC3B siRNA (C) within the lipid matrix.

To evaluate the biological activity of the encapsulated siRNA, APOBEC3B mRNA expression was quantified by RT-qPCR in MDA-MB-231 cells treated with siRNA (C)-NLCs, free siRNA (C), blank NLCs, and a non-targeting siRNA negative control (Fig. 3-C). No significant difference in APOBEC3B expression was observed between the mock control and either blank NLC-treated cells ($p = 0.5242$) or the negative control group ($p = 0.9972$). In contrast, both siRNA (C)-NLCs and free siRNA (C) significantly reduced APOBEC3B mRNA expression compared with the mock control ($p < 0.0001$). Treatment with siRNA (C)-NLCs resulted in a $2^{-\Delta\Delta Cq}$ value of 0.030, corresponding to approximately 97.0% gene silencing (mean difference from mock = 0.8910; 95% CI: 0.748–1.034), while free siRNA.

4.2.3. Box Behnken design (BBD)

The BBD was employed to identify the impact of independent variables (GMS, Labrasol and Tween 80) on the dependent variables (% EE and particle size). Based on the screening studies, these three variables were identified as crucial parameters, and their quantities were varied at three levels. A total of 15 runs are mentioned in Table 2. The optimised formulation was evaluated from BBD and characterised for all parameters. The R^2 value was found using ANOVA to understand the degree of deviation from the average, and the *p*-value was determined to analyse the significance of the difference among them.

4.2.3.1. Effect of independent variables on entrapment efficiency. The influence of glyceryl monostearate (GMS, A), Labrasol (B), and Tween 80 (C) on the entrapment efficiency (% EE) (Y1) of Gem HCl-NLCs was evaluated using a three-factor, three-level Box-Behnken Design. The experimental %EE values ranged from 42.74% to 74.13%, demonstrating a substantial effect of formulation variables on drug encapsulation. The highest entrapment efficiency (74.13%) was obtained in formulation F11 (240 mg GMS, 180 mg Labrasol, 400 mg Tween 80), whereas the lowest value (42.74%) was observed in formulation F7 (80 mg GMS, 60 mg Labrasol, 400 mg Tween 80).

The quadratic polynomial equation described the relationship between formulation variables and % EE: $Y1 = 67.37 + 5.84\,A + 9.77\,B - 4.21C - 3.12\,AB - 0.7275\,AC - 0.1250\,BC - 2.94\,A^2 - 2.87\,B^2 - 4.69\,C^2$.

The model demonstrated good agreement with the experimental data, with an R^2 value of 0.9031 and a predicted R^2 of 0.8061. Analysis of variance confirmed the statistical significance of the model ($p < 0.05$). Among the formulation variables, Labrasol exhibited the most significant positive effect on % EE ($P = 0.0036$), followed by GMS ($P = 0.0277$), while Tween 80 showed a negative but statistically non-significant influence. Three-dimensional response surface plots illustrating the effects of formulation variables on % EE are presented in Fig. 3-D.

4.2.3.2. Effect of independent variables on particle size. Particle size (PS) (Y2) of Gem HCl-NLCs was also significantly influenced by the formulation variables investigated. Experimental particle size ranged from 140.21 nm (F6) to 222.17 nm (F2), with all formulations remaining within the nanometric range suitable for drug delivery applications. The relationship between independent variables and particle size was represented by the following quadratic polynomial equation:

$$Y_2 = 185.11 + 6.35\,A + 8.68\,B - 30.61C - 3.57\,AB + 1.21\,AC - 6.38\,BC - 8.09\,A^2 - 5.13\,B^2 + 1.90\,C^2.$$

The model exhibited excellent predictive capability, with an R^2 value of 0.9566 and a predicted R^2 value of 0.7954. Analysis of variance demonstrated that the model was statistically significant ($p < 0.05$), with low experimental variability (% CV = 5.04). Tween 80 showed the most significant influence on particle size ($p = 0.0002$), while Labrasol also significantly affected particle size ($p = 0.0417$). GMS exhibited a positive but statistically non-significant effect. The three-dimensional response surface plot illustrating the effect of formulation variables on particle size is shown in Fig. 3-D.

4.3. Characterisation studies

4.3.1. Particle size & entrapment efficiency

Gem HCl and APBEC3B siRNA (C) were co-loaded into NLCs using the hot microemulsification method. The formulation consisted of 2% total lipid with a lipid ratio of 4:3:3 (GMS: Labrasol: Phosphatidylcholine), optimised through BBD. Among the experimental formulations, the optimised composition corresponding to experimental run 9, containing GMS (240 mg), Labrasol (180 mg), Tween 80 (400 mg), and phosphatidylcholine (120 mg), was selected for further characterisation.

The optimised Gem HCl: APOBEC3B siRNA (C)-NLCs exhibited a mean particle size of 188.2 ± 4.6 nm, a PDI of 0.284 ± 0.03, and a zeta potential of −3.30 ± 1.6 mV (Fig. 4-A). Entrapment efficiency analysis

Table 2
Matrix and response values for the BBD for Gem HCl-NLCs optimisation using Design-Expert 13 software.

Experimental run	Independent variables			Dependent variables	
	X1 (GMS, mg)	X2 (Labrasol, mg)	X3 (Tween 80, mg)	Y1 (Percent entrapment, %EE)	Y2 (Particle size, nm)
1	160	120	400	68.54 ± 2.04	198.23 ± 2.36
2	160	180	200	71.67 ± 3.16	222.17 ± 3.12
3	240	120	200	72.68 ± 2.98	215.21 ± 3.47
4	160	120	400	65.21 ± 3.12	180.53 ± 2.29
5	240	120	600	55.56 ± 2.67	152.14 ± 3.68
6	80	120	600	48.26 ± 3.23	140.21 ± 2.19
7	80	60	400	42.74 ± 2.46	148.43 ± 2.78
8	240	60	400	63.58 ± 3.23	171.46 ± 3.89
9	160	120	400	68.36 ± 3.19	176.58 ± 2.87
10	160	60	200	49.12 ± 2.19	198.56 ± 3.32
11	**240**	**180**	**400**	**74.13** ± 3.37	**188.20** ± 2.56
12	80	180	400	65.78 ± 2.85	179.46 ± 2.78
13	80	120	200	62.47 ± 3.61	208.12 ± 3.19
14	160	180	600	70.26 ± 2.94	152.45 ± 2.60
15	160	60	600	53.17 ± 2.89	154.35 ± 3.18

demonstrated successful incorporation of both therapeutic agents, with Gem HCl exhibiting an entrapment efficiency (% EE) of 74.13 ± 3.37% and a drug loading (DL %) of 3.44 ± 1.12%. APOBEC3B siRNA (C) exhibited an entrapment efficiency of 61.32 ± 2.84%. These findings confirm the successful development of a Gem HCl: APOBEC3B siRNA (C)-NLCs system with nanoscale particle size and substantial encapsulation of both drug and siRNA.

4.3.2. Surface modification of NLCs using hyaluronic acid (HA)

To identify the most suitable coating condition, the physicochemical characteristics of the evaluated formulations were compared. Among the formulations investigated, the NLC formulation with a mass ratio of 3:1, prepared using 0.05% HA (0.5 mg/mL), exhibited the most favourable physicochemical properties, including a smaller particle size and moderate PDI compared with the other formulations (Table 3). Increasing the HA concentration and changing the NLC mass ratio from 3:1 to 1:3 resulted in a progressive increase in particle size, reaching approximately 589 nm in the formulation with the highest HA concentration. Concurrently, the zeta potential became increasingly negative with increasing HA concentration. Some formulations also exhibited higher polydispersity index (PDI) values, indicating greater particle size heterogeneity and a less uniform particle size distribution.

Surface modification of the optimised Gem HCl: APOBEC3B siRNA (C)-NLCs was subsequently performed using 0.05% HA (0.5 mg/mL). Following HA coating, the particle size increased from 188.2 nm for the uncoated NLCs to 278.7 nm, as determined by dynamic light scattering (DLS). In addition, the zeta potential shifted substantially from −3.30 mV to −35.3 mV, accompanied by a low PDI value of 0.137 (Fig. 4-B). These changes indicate successful HA adsorption onto the NLC surface, as evidenced by the increase in particle size and the shift towards a more negative surface charge. The low PDI further suggests a relatively narrow particle size distribution, while the more negative zeta potential is consistent with improved electrostatic repulsion between particles, potentially contributing to enhanced colloidal stability.

Transmission electron microscopy (TEM) was used to directly assess individual particle geometry and morphology, with quantitative size measurements performed in ImageJ on the micrographs. TEM image (Fig. 4D) revealed spherical nanoparticles with an electron-dense lipid core surrounded by a distinct, diffuse peripheral HA layer, providing direct evidence of HA surface coating with no visible aggregation, confirming structural integrity and colloidal stability. The TEM-derived mean particle diameter was 163.88 nm, which is expectedly smaller than the DLS hydrodynamic diameter of 278.7 nm, as DLS measure particle diameter in solution, inclusive of the hydration layer and HA surface coating, whilst TEM reflects the diameter of individual particles in the dried state.

The stability study results revealed that the change in formulation was negligible when observed with the naked eye after 28 days of storage. The outcomes are illustrated in Fig. 5A-D; parameters of Gem HCl NLCs, siRNA-NLCs, Gem HCl:siRNA-NLC and HA-Gem HCl-NLC fluctuated within a certain range, but within acceptable limits, which indicates that the formulation was stable for 28 days and maintained the integrity of both cargoes.

4.3.2.1. FTIR spectroscopy. FTIR spectroscopy was performed to investigate the compatibility of formulation components and to confirm the successful incorporation of Gem HCl and HA coating within the NLC system. The FTIR spectrum of Gem HCl exhibits peaks at 3384 cm^{-1} (O-H/N-H stretching), 3076 cm^{-1} (C—H stretching), 1673 cm^{-1} (C═O stretching), and peaks between 1533 cm^{-1} and 1196–1060 cm^{-1} (amide and C—O functional groups). The FTIR spectrum of HA has a large peak at 3201 cm^{-1} (O—H stretching), a peak at 1604 cm^{-1} (carboxylate C═O stretching), and a strong band near 1030 cm^{-1} (C-O-C stretching), Fig. 4E.

The FTIR spectrum of HA-Gem HCl NLCs retained the characteristic absorption bands of both Gem HCl and HA; however, several peaks exhibited broadening and slight shifts. In particular, the O—H stretching band shifted to 3270 cm^{-1}, while the carbonyl stretching band shifted to 1636 cm^{-1}. A reduction in the intensity of several characteristic peaks and partial peak overlap was also observed in the coated NLC formulation. No new absorption bands appeared, and none of the major characteristic peaks of Gem HCl or HA disappeared following formulation and surface modification.

4.3.3. Evaluation studies

4.3.3.1. In vitro drug release and release kinetics. The *in vitro* release profile of APOBEC3B siRNA and Gem HCl was evaluated in PBS pH 7.4 and compared between the free drug solution and the NLC-based formulation. Free siRNA and Gem HCl exhibited rapid release characteristics, with approximately 68.37% and 58.16% release, respectively, within the first hour. Nearly complete release of both agents was observed within 3–6 h, indicating immediate diffusion into the release medium in the absence of a carrier system. In contrast, NLC-based formulations demonstrated markedly sustained release behaviour. The initial release during the first hour was significantly reduced for siRNA-NLC (28.35%), Gem HCl-NLC (30.46%), and HA-Gem HCl: siRNA-NLCs (20.31%), indicating suppression of the burst release effect following encapsulation. After 72 h, cumulative release reached approximately 99.02% for siRNA-NLC, 98.00% for Gem HCl-NLC and 89.00% for HA-Gem HCl: siRNA-NLCs (Fig. 6). Among all formulations, HA-Gem HCl: siRNA-NLCs exhibited the slowest release profile.

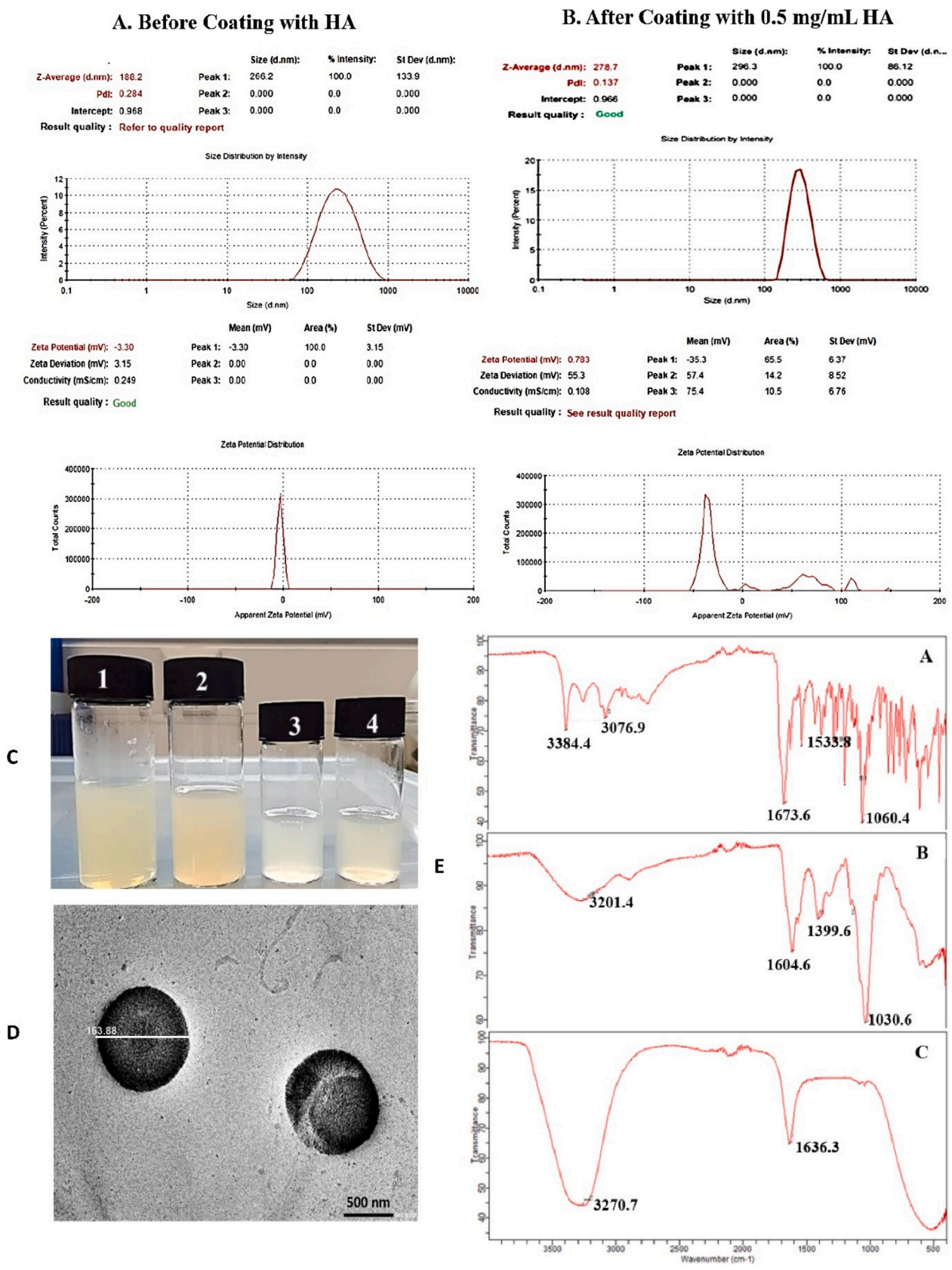

Fig. 4. Dynamic light scattering (DLS) analysis showing particle size, PDI and zeta potential distribution of (A) Gem HCl: APOBEC3B siRNA (C)-NLCs before HA coating and (B) HA-Gem HCl: APOBEC3B siRNA (C)-NLCs (0.5 mg/mL HA). The measurement illustrates the effect of HA coating on particle size, PDI, and surface charge of the optimised formulation. (C) Formulations: (1) Blank NLCs; (2) Gem HCl: siRNA-NLCs; (3) HA-coated NLCs; (4) HA-Gem HCl: siRNA-NLCs. (D) TEM image of HA-drug-loaded NLCs revealing spherical morphology, smooth surface characteristics, and homogeneous particle dispersion. (E) FTIR spectra of Gem HCl (A), hyaluronic acid (B), and HA-Gem HCl: siRNA-NLCs (C) using an attenuated total reflectance accessory by FTIR-NICOLET™ SUMMIT™.

Table 3
NLC:HA mass ratio for the surface modification.

NLC:HA (mass ratio)	HA required (mg)	0.05% (0.5 mg/mL)	0.10% HA (1.0 mg/mL)	0.15% (1.5 mg/mL)	0.20% (2.0 mg/mL)
3:1	13.33 mg	26.67 mL SIZE: 232.32 nm PDI: 0.356 ZETA: −35.3	13.33 mL SIZE: 342 nm PDI: 0.242 ZETA: −43.7	8.89 mL SIZE: 417 nm PDI: 0.212 ZETA: −55.1	6.67 mL SIZE: 589 nm PDI: 0.466 ZETA: −52.7
2:1	20.00 mg	40.00 mL SIZE: 426 nm PDI: 0.187 ZETA: −39.3	20.00 mL SIZE: 449 nm PDI: 0.18 ZETA: −43.4	13.33 mL SIZE: 556 nm PDI: 0.209 ZETA: −44.3	10.00 mL SIZE: 582 nm PDI: 0.303 ZETA: −43.3
1:1	40.00 mg	80.00 mL SIZE: 446 nm PDI: 0.212 ZETA: −38.3	40.00 mL SIZE: 456 nm PDI: 0.312 ZETA: −41.4	26.67 mL SIZE: 455 nm PDI: 0.281 ZETA: −44.3	20.00 mL SIZE: 466 nm PDI: 0.342 ZETA: −44.7
1:2	80.00 mg	160.00 mL SIZE: 387 nm PDI: 0.235 ZETA: −40.2	80.00 mL SIZE: 390 nm PDI: 0.214 ZETA: −44.3	53.33 mL SIZE: 410 nm PDI: 0.321 ZETA: −45.4	40.00 mL SIZE: 414 nm PDI: 0.285 ZETA: −45.6
1:3	120.00 mg	240.00 mL SIZE: 380 nm PDI: 0.322 ZETA: −39.3	120.00 mL SIZE: 415 nm PDI: 0.276 ZETA: −42.3	80.00 mL SIZE: 424 nm PDI: 0.345 ZETA: −45.5	60.00 mL SIZE: 467 nm PDI: 0.244 ZETA: −44.6

To elucidate the release mechanism, the experimental data were fitted to zero-order, first-order, Higuchi, and Korsmeyer-Peppas kinetic models. Comparative analysis of the correlation coefficient (R^2) indicated that the Korsmeyer-Peppas model provided the best fit to the release data, with an R^2 of 0.925. The release exponent (n) obtained from the model was 0.65. The n value was determined from the slope of the linear plot of log cumulative drug release *versus* log time ($Mt/M\infty = ktn$), which characterises the mechanism of drug release. According to established criteria, $n < 0.45$ indicates Fickian diffusion, $0.45 < n < 0.89$ indicates anomalous (non-Fickian) transport, and $n > 0.89$ suggests case-II transport, involving erosion- or relaxation-controlled mechanisms.

4.3.3.2. Cytotoxicity assay. The cytotoxic effect of plain Gem HCl, Gem HCl-NLCs, and bank NLCs against MDA-MB-231 cells was evaluated at 24, 48, and 72 h using dose-response analysis. At 24 h, plain Gem HCl exhibited pronounced cytotoxic activity with an IC_{50} value of 27.13 μM. Whereas Gem HCl-NLCs displayed a comparatively higher IC_{50} value of 49.44 μM (Fig. 7-A), Blank NLCs demonstrated minimal cytotoxicity, with an IC_{50} value of 172.6 μM. Following 48 h of treatment, the IC_{50} values of both formulations decreased substantially, reaching 9.49 μM for plain Gem HCl and 13.95 μM for Gem HCl-NLCs. A further reduction in IC_{50} was observed at 72 h, with values of 5.46 μM and 9.15 μM for plain Gem HCl and Gem HCl-NLCs, respectively. Blank NLCs continued to exhibit negligible toxicity, with an IC_{50} value of 102.2 μM at 72 h.

The cytotoxicity of APOBEC3B siRNA was assessed independently over the same incubation period (Fig. 7-B). Cell viability remained between 96% and 100% at 24 h across the tested concentration range. At 48 h, cell viability remained above 69% even at the highest concentration evaluated (100 pmol). Following 72 h of exposure, approximately 51% cell viability was observed at 100 pmol, indicating only a modest reduction in viability with prolonged incubation. Overall, APOBEC3B siRNA treatment did not induce substantial cytotoxicity in MDA-MB-231 cells throughout the study.

Further, the cytotoxic effect of various treatment groups on MDA-MB-231 cells was evaluated following RNAiMAX-mediated transfection at 24 and 48 h (Fig. 7-C). The mock group maintained approximately 100% cell viability throughout the study, indicating normal cellular growth and proliferation. Lipofectamine-treated cells exhibited only a slight reduction in viability, with values of 96.45% and 91.45% at 24 and 46 h, respectively. Similarly, blank NLCs and APOBEC3B siRNA (C)-NLCs maintained high cell viability (>80%) at both time points, indicating minimal cytotoxicity.

In contrast, Gem HCl-NLCs produced a substantial decrease in cell viability, reducing survival to 71.35% at 24 h and 62.67% at 48 h. A further reduction was observed in cells treated with Gem HCl: APOBEC3B siRNA-NLCs, which exhibited viabilities of 64.56% and 51.38% at 24 and 48 h, respectively. HA-Gem HCl: APOBEC3B siRNA-NLCs showed the greatest cytotoxic effect, with cell viabilities of 52.46% and 38.56% at 24 and 48 h, respectively.

One-way ANOVA revealed a significant difference among treatment groups ($F(6,7) = 19.93$, $P = 0.0005$). Subsequently, Dunnett's multiple comparison test demonstrated that lipofectamine, blank NLCs and APOBEC3B siRNA (C)-NLCs were not significantly different from the mock control ($p > 0.05$). Conversely, Gem HCl-NLCs significantly reduced cell viability compared with the mock group ($p = 0.0053$). A more pronounced reduction was observed for Gem HCl: APOBEC3B siRNA-NLCs ($p = 0.0013$), while HA-Gem HCl: APOBEC3B siRNA-NLCs exhibited the highest level of statistical significance ($p = 0.0003$).

4.3.3.3. Cell migration assay. The effect of different formulations on the migratory behaviour of MDA-MB-231 cells was evaluated using a wound-healing assay at 12 and 24 h (Fig. 8-A). At 12 h, untreated control cells exhibited rapid wound closure, achieving 49.26% wound coverage, indicative of the highly migratory phenotype of MDA-MB-231 cells. Blank NLC-treated cells displayed a comparable migration pattern, with 38.61% wound coverage, suggesting minimal influence of the carrier system on cellular motility. Treatment with free Gem HCl reduced wound closure to 24.76%, whereas Gem HCl-NLCs resulted in 29.35% wound coverage. Among all treatment groups, HA-Gem HCl siRNA-NLCs demonstrated the greatest inhibition of migration, exhibiting only 30.23% wound coverage at 12 h.

A more pronounced inhibition of migration was observed after 24 h of treatment. Untreated control cells achieved 90.13% wound closure, while blank NLC-treated cells showed 73.54% wound coverage. Free Gem HCl reduced wound closure to 36.97%, whereas Gem HCl-NLCs exhibited comparable suppression of migratory activity. Notably, HA-Gem HCl: siRNA-NLCs reduced the strongest anti-migratory effect, with wound closure limited to 39.41%. Compared with untreated control cells, the HA-Gem HCl siRNA-NLCs reduced wound closure by approximately 56.3% after 24 h, representing the most effective inhibition of cell migration among all treatment groups (Fig. 8-B).

4.3.3.4. Intracellular uptake studies. Confocal laser scanning microscopy (CLSM) was employed to investigate the intracellular uptake of rhodamine B-loaded NLCs and HA-coated rhodamine B-loaded NLCs in MDA-MB-231 cells. Rhodamine B was used as a hydrophilic fluorescent probe to replace Gem HCl and APOBEC3B siRNA for visualisation of nanoparticle internalisation. Following incubation at 37 °C for 1 and 2 h, both formulations exhibited successful cellular uptake, as evidenced by the presence of strong orange-yellow fluorescence signals corresponding to rhodamine B within the cells, while nuclei were distinctly stained blue with DAPI (Fig. 9).

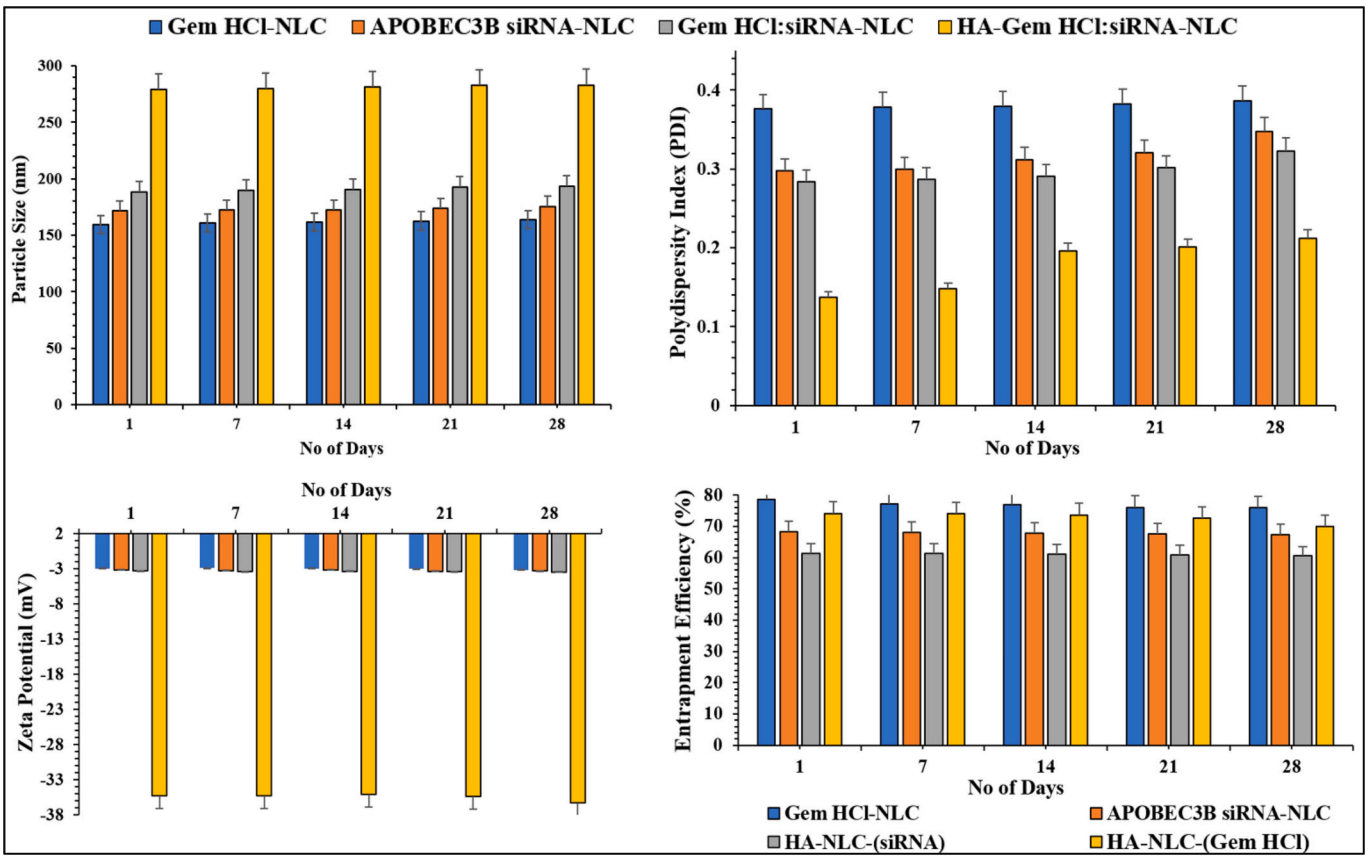

Fig. 5. Physicochemical stability profiles of Gem CL-NLCs, APOBEC3B siRNA-NLCs, Gem HCl: siRNA-NLCs, and HA-Gem HCl:siRNA-NLCs over 28 days of storage at 4 °C, assessed by (A) particle size (nm), (B) polydispersity index (PDI), (C) zeta potential (mV), and (D) entrapment efficiency (%). All formulations demonstrated no statistically significant changes in particle size, PDI, zeta potential, or entrapment efficiency throughout the study period, confirming colloidal integrity and physicochemical stability of the developed nanoformulation over 28 days. Data represent mean ± SEM ($n = 3$).

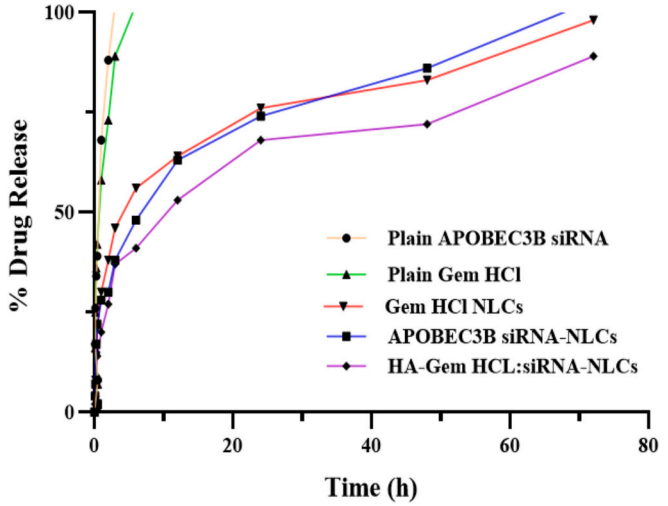

Fig. 6. *In vitro* cumulative release profiles of plain Gem HCl, plain APOBEC3B siRNA, Gem HCl-NLCs, APOBEC3B siRNA-NLCs, and HA-Gem HCl: siRNA-NLCs in PBS (pH 7.4) over 72 h. The NLC formulations exhibited sustained release compared with the plain drug and siRNA, while HA coating on NLCs further prolonged the release profile. Data are presented as mean ± SD ($n = 3$).

For rhodamine B-loaded NLCs, fluorescence intensity increased from 1 to 2 h, indicating progressive time-dependent cellular internalisation. Notably, HA-coated rhodamine B-loaded NLCs exhibited substantially greater fluorescence intensity at both time points compared with uncoated NLCs. The fluorescence signal was broadly distributed throughout the cytoplasm, with partial accumulation in the perinuclear region. Minimal extracellular fluorescence and negligible nanoparticle aggregation were observed for either formulation (Fig. 9).

Fluorescence intensity analysis revealed a significant time-dependent increase in intracellular Rhodamine B signal for both NLC formulations between 1 and 2 h. RhB-NLCs demonstrated progressively greater intracellular fluorescence at 2 h compared with 1 h (mean: 84.1 ± 8.1 *vs* 64.3 ± 7.1 a.u.), whilst HA-coated NLCs showed concentrated perinuclear accumulation at 2 h consistent with active endosomal trafficking following CD44-mediated internalisation. One-way ANOVA confirmed a significant overall effect of formulation and time on intracellular fluorescence intensity ($F = 5.26$, $p = 0.002$). The qualitative increase in intracellular fluorescence density observed for both formulations at 2 h relative to 1 h, and the more homogeneous cytoplasmic distribution observed with HA-coated NLCs, are consistent with CD44 receptor-mediated active internalisation of the HA-functionalised nanoparticles in MDA-MB-231 cells.

4.3.3.5. In vitro apoptosis assay. Annexin V-FITC/PI flow cytometric analysis of MDA-MB-231 cells following 24 h of treatment showed distinct apoptotic profiles across all experimental groups. The untreated control maintained high viability (89%), with only 2.9% early and 7.4% late apoptosis, indicating normal cellular viability (Fig. 10-A). Blank NLC-treated cells similarly retained high viability (84.9%), with limited early (4.8%) and late apoptotic (10.4%) populations, confirming carrier biocompatibility, further supported by Dunnett's multiple comparison test, which showed no statistically significant difference in viable cell population between blank NLC and control ($p = 0.9781$). Free Gem HCl

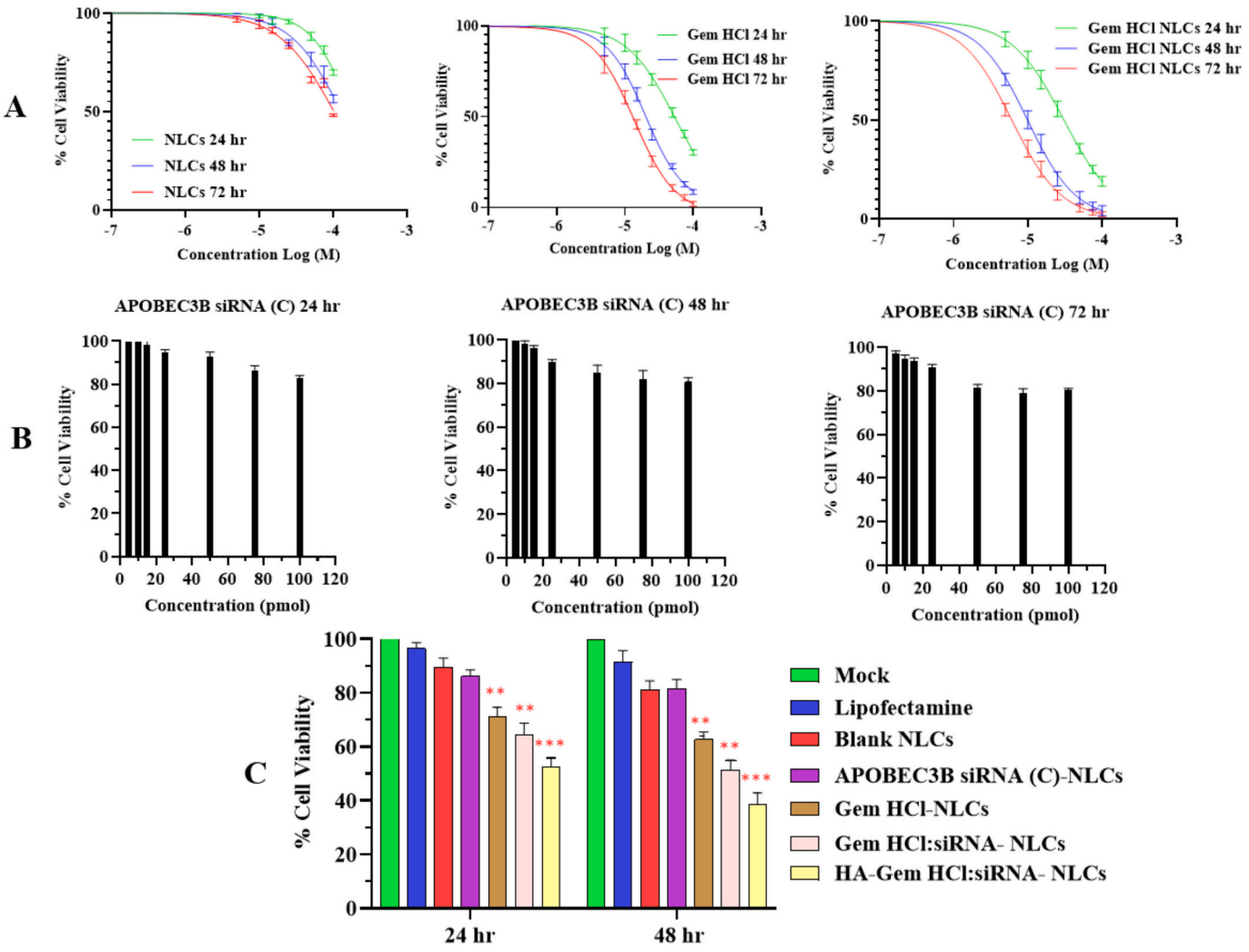

Fig. 7. *In vitro* cytotoxicity and transfection efficiency of Gem HCl and APOBEC3B siRNA in MDA-MB-231 cells. (A) Dose-dependent cytotoxicity of free Gem HCl following 24, 48, and 72 h of treatment, determined by the MTT assay. (B) Dose-dependent cytotoxicity of APOBEC3B siRNA at different concentrations (pmol) after 24, 48, and 72 h. (C) Cytotoxicity of APOBEC3B siRNA delivered using Lipofectamine RNAiMAX under different treatment conditions following 24 and 48 h of treatment. Cell viability was expressed as a percentage relative to untreated control cells. Data are presented as mean ± SD ($n = 3$). Statistical significance was determined by one-way ANOVA followed by Dunnett's multiple comparison test (**$p < 0.01$, ***$p < 0.001$ *vs* control).

markedly increased total apoptosis to 52.8% (early: 11.6% and late: 41.2%), with viable cells reduced to 47.2%, consistent with its established cytotoxic mechanism of DNA synthesis inhibition and apoptosis induction in rapidly proliferating tumour cells. Gem HCl-NLCs also induced a total apoptosis of 35.5% (early: 9.5% and late: 26.0%), with 64.5% viable cells remaining, reflecting controlled and sustained Gem HCl release from the NLC matrix relative to the immediate availability of free drug.

The Gem HCl: APOBEC3B siRNA-NLC group demonstrated a total apoptosis of 50.2% (early: 6.1% and late: 44.1%), with 49.8% viable cells, indicating enhanced apoptotic induction attributable to combined NLC-mediated drug-gene co-delivery without active CD44 targeting, notably superior to Gem HCl-NLCs alone (36.5%), confirming the additive contribution of APOBEC3B gene silencing to the apoptotic response. HA-Gem HCl: APOBEC3B siRNA-NLCs induced a total apoptosis of 47.8% (early: 7.2%; late: 40.6%), with viable cells reduced to 52.2%, substantially greater than Gem HCl-NLCs (35.5%), blank NLCs (15.2%) and the untreated control, confirming the sustained and progressive anti-tumour effect of the HA-functionalised co-loaded formulation. Dunnett's multiple comparison test confirmed that all active treatment groups produced a statistically significant reduction in viable cell population relative to the untreated control ($p < 0.0001$).

4.3.3.6. Cell cycle distribution assay. The effect of different formulations on cell cycle progression in MDA-MB-231 cells was evaluated after 24 h of treatment using flow cytometric analysis (Fig. 10-B). The untreated control group exhibited a typical cell cycle distribution, with the majority of cells residing in the G0/G1 phase (90.1%), followed by the S phase (4.7%) and G2/M phase (2.5%). A small Sub-G1 population (2.7%) was also observed, representing the basal level of apoptotic cells. Similarly, blank NLC-treated cells showed a comparable cell cycle profile with 89.1% of cells in the G0/G1 phase, 7.8% in the S phase, and 6.0% in the G2/M phase, indicating that the carrier system did not significantly alter normal cell cycle progression.

Free Gem HCl produced the highest acute G2/M accumulation (52.3%) with a corresponding G0/G1 reduction (32.9%) and Sub-G1 fraction of 6.3%, consistent with ribonucleotide reductase inhibition and DNA replication. Gem HCl-NLCs induced attenuated G2/M arrest (27.2%) with elevated Sub-G1 (10.29%), reflecting controlled intracellular drug release relative to free drug. The Gem HCl: APOBEC3B siRNA-NLC group demonstrated 31.1% G2/M accumulation with a notably elevated S-phase population (14,9%), indicating enhanced replication stress without CD44-mediated active targeting compared to Gem HCl-NLCs. HA-Gem HCl: APOBEC3B siRNA-NLC produced 26.3% G2/M accumulation, the lowest S-phase population across all groups (4.4%),

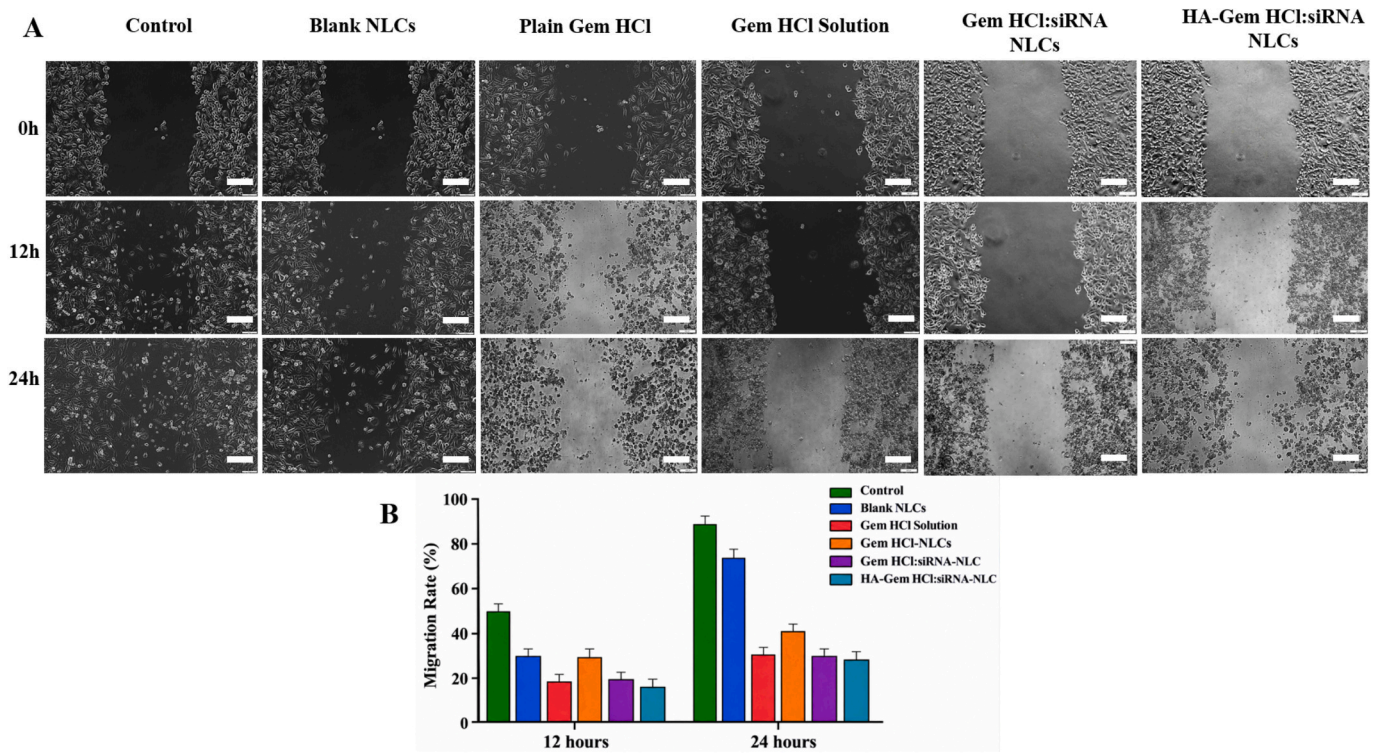

Fig. 8. *In vitro* wound healing assay showing the effect of different formulations on the migratory ability of MDA-MB-231 cells. (A) Representative phase-contrast images of wound closure in control, blank NLCs, free Gem HCl, Gem HCl-NLCs, and HA-Gem HCl: APOBEC3B siRNA-NLCs at 0, 12, and 24 h following scratch formation (Scale bar: 200 μm). (B) Quantitative analysis of the percentage cell migration (wound closure) at the corresponding time points. Treatment with HA-Gem HCl: APOBEC3B siRNA-NLCs showed the greatest inhibition of cell migration compared with the other treatment groups. Data are presented as mean ± SD ($n = 3$).

and an elevated Sub-G1 fraction (7.9%), alongside the greatest G0/G1 reduction among all NLC formulations (Fig. 10-B), indicating sustained response rather than inferior activity due to HA coating, which retards Gem HCl release and produces a controlled intracellular drug exposure profile that distributes cell cycle disruption progressively beyond the 24-h observation.

Dunnett's multiple comparison test showed that blank NLCs showed only a slight reduction in the G0/G1 population (mean difference = 3.60%, $p = 0.0304$). In contrast, other treated formulations significantly decreased the proportion of cells in the Go/G1 phase compared with the control ($p < 0.05$), with the greatest reduction observed for Gem HCl (mean difference = 52.81%), followed by HA-Gem HCl: APOBEC3B siRNA-NLCs (37.97%) and Gem HCl-NLCs (35.91%) (Fig. 10-D), indicating treatment-induced cell cycle distribution.

4.3.4. Chorioallantoic membrane (CAM) assay

4.3.4.1. Optimisation of tumour formation and embryo survival. Of the 36 eggs allocated across three independent biological replicates, 25 survived to E14 (69% embryo survival rate), with mortality attributable to low haemoglobin and mechanical stress during windowing and cell implantation. The distribution of surviving eggs across treatment groups was as follows: untreated control (9 surviving); free Gem HCl (8 surviving); HA-Gem HCl: APOBEC3B siRNA-NLCS (8 surviving). Pre-treatment of the CAM surface with trypsin prior to MDA-MB-231 cell inoculation markedly improved tumour engraftment, with successful tumour formation confirmed in approximately 14 of 36 allocated eggs (39% engraftment rate). Tumour nodules became macroscopically visible beneath the CAM surface within 3–4 days post-implantation and progressively increased in size, reaching approximately 1–5 mm in diameter by embryonic day 11 (E11). A notable observation was that embryos exhibiting relatively low heartbeat activity on embryonic day 3 demonstrated a higher frequency of successful tumour establishment compared with embryos displaying more vigorous circulation. Following successful engraftment, tumour xenografts developed an extensive vascular network originating from the surrounding CAM vasculature. Newly formed blood vessels infiltrated the tumour mass and established a dense microvascular architecture capable of supporting tumour growth. Histological examination confirmed the presence of invasive tumour tissue exhibiting morphological features characteristic of TNBC, with tumour architecture closely resembling that of human breast tumour specimens.

4.3.4.2. Effect of HA-Gem HCl: APOBEC3B siRNA-NLCs on CAM. The MDA-MB-231 CAM xenograft model was used to assess preliminary treatment-associated changes in tumour appearance. Treatments were administered on embryonic day 11 (E11), and tumours were harvested on E14. Representative macroscopic images (Fig. 11-1) showed differences in tumour morphology between the control, free Gem HCl and HA-Gem HCl: APOBEC3B siRNA-NLC-treated groups. The combination-treated tumours appeared smaller and less prominent than those in the control and free Gem HCl groups. However, in the absence of quantitative tumour measurement, these observations remain preliminary and cannot establish statistically significant tumour growth inhibition.

Tumour area and vascular density were quantified from representative stereomicroscopic images using ImageJ software. At E11, tumour areas across all groups were comparable (0.117–0.538 mm^2) (Fig. 11-2), reflecting inherent biological variability in CAM engraftment. By E14, the untreated control demonstrated marked tumour progression (1.676 ± 0.073 mm^2) with dense vascular density (30.54 ± 1.28%) (Fig. 11-3), confirming active tumour-driven angiogenesis. Free Gem HCl produced substantial tumour suppression (0.097 ± 0.004 mm^2; TGI = 94.2%) with significantly reduced vascular density (11.54 ± 0.48%; $p < 0.001$ *vs* control). HA-Gem HCl: APOBEC3B siRNA-NLCs similarly achieved marked tumour regression (0.182 ± 0.008 mm^2; TGI = 89.1%), with

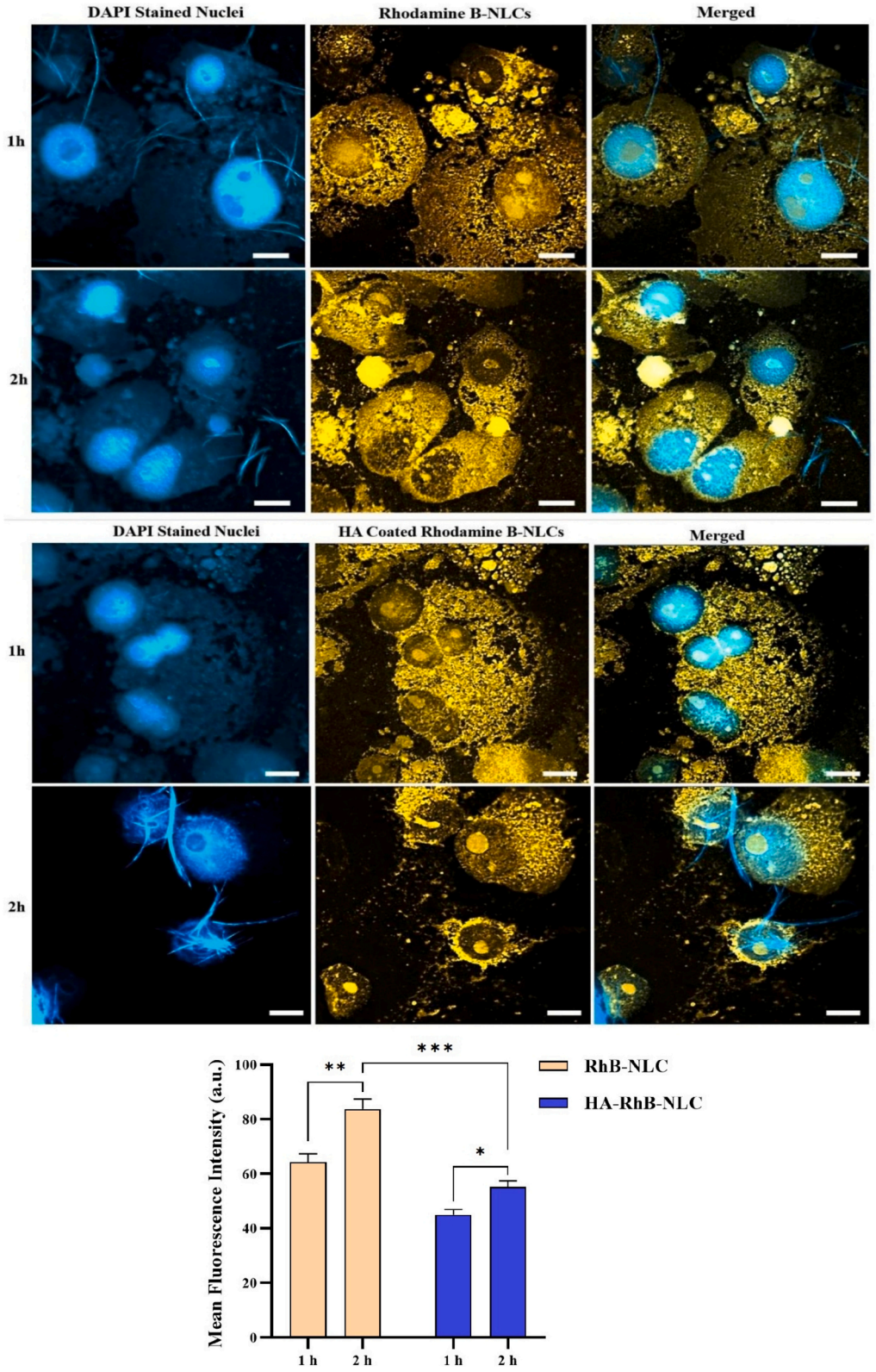

Fig. 9. Cellular uptake of Rhodamine B-loaded NLCs and HA-coated Rhodamine B-loaded NLCs by MDA-MB-231 cells following exposure at 37 °C for 2 h. DAPI-stained nuclei (blue; excitation 347 nm, emission 483 nm) are overlaid with Rhodamine B fluorescence (orange-yellow; excitation 540–560 nm, emission 570–590 nm). Intracellular fluorescence intensity was quantified by CTCF analysis using ImageJ software; data represent mean ± SEM. Statistical significance was determined by one-way ANOVA ($F = 5.26$, $p = 0{,}002$) with Welch *t*-test pairwise comparison; $^{**}p < 0.01$, $^{***}p < 0.001$. HA-coated NLCs demonstrated significantly greater intracellular fluorescence accumulation at 2 h compared with uncoated NLCs ($p < 0.001$), consistent with CD44 receptor-mediated active internalisation. All scale bars: 50 μm. Magnification: ×63.

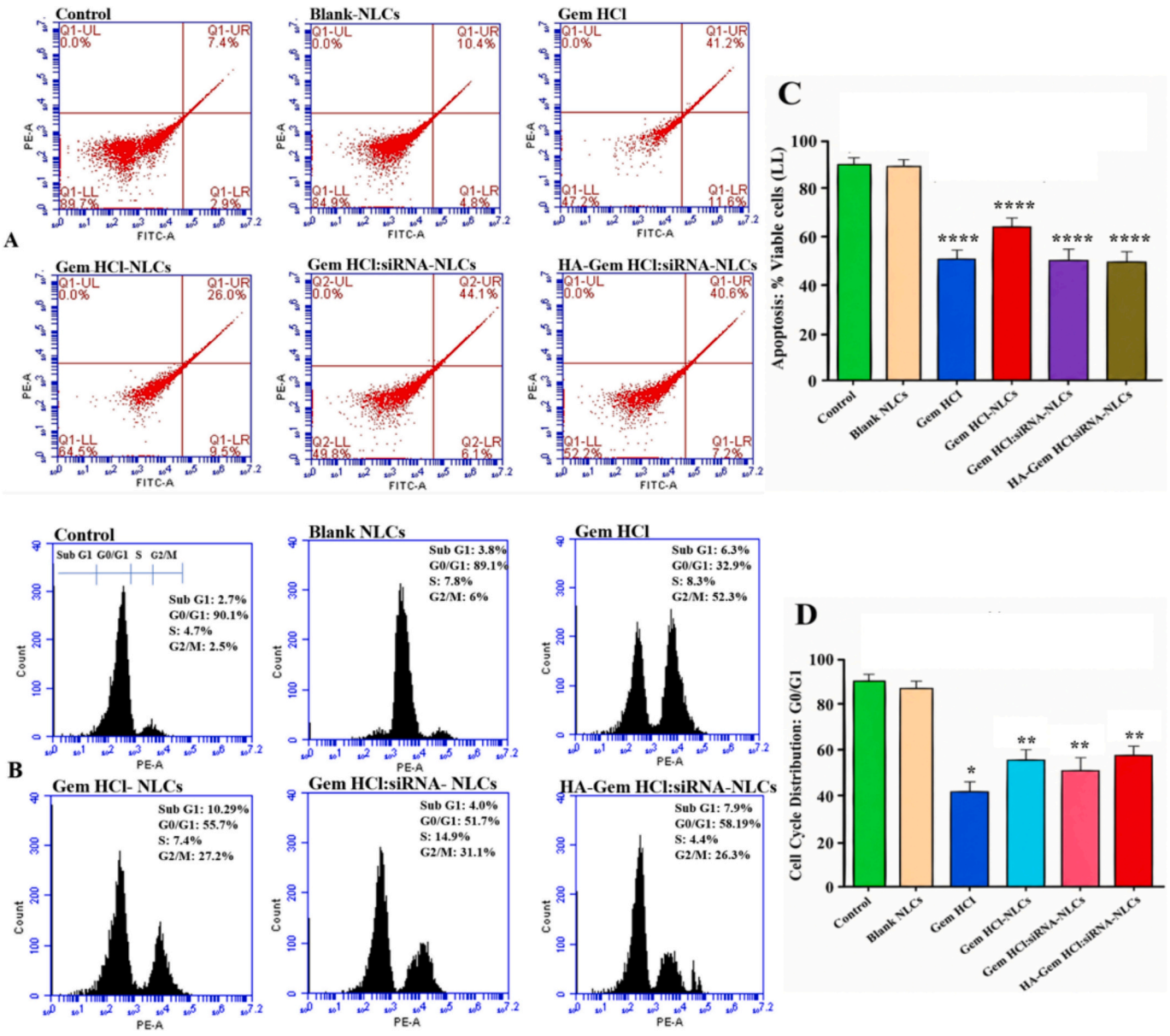

Fig. 10. (A) Representative flow cytometry plots of Annexin V-FITC/PI double staining showing the distribution of viable, early apoptotic, late apoptotic, and necrotic cells following treatment with control, blank NLCs, free Gem HCl, Gem HCl-NLCs, Gem HCl: siRNA-NLCs, and HA-Gem HCl: APOBEC3B siRNA-NLCs. (B) Cell cycle distribution analysis demonstrating the effect of the different formulations on the percentage of cells in the G0/G1, S, G2/M, and sub-G1 phases. The HA-Gem HCl: APOBEC3B siRNA-NLCs formulation induced the greatest apoptosis and cell cycle arrest compared with the other treatment groups. (C–D) represent quantitative analysis of viable cells (LL) and G0/G1 cell cycle distribution in MDA-MB-231 cells following treatment. Blank NLCs showed no significant effect on cell viability and only a minimal effect on G0/G1 distribution, whereas all treatment groups significantly reduced viable cells and the G0/G1 population compared with the untreated control (Dunnett's multiple comparison test). Data are presented as mean ± SD ($n = 3$). *$P < 0.05$; **$P < 0.01$; ****$P < 0.0001$.

both treatment groups demonstrating statistically significant tumour suppression relative to control ($p < 0.001$; one-way ANOVA, Dunnett's post-hoc). Whilst whole-image vascular density analysis yielded an elevated value for HA-NLC at E14 (39.35 ± 1.64%), attributable to prominent peripheral CAM vessels captured by whole-image thresholding rather than tumour-associated neovascularisation. Tumours in the HA-NLC group on E14 were significantly smaller than at E11, the control group and those receiving Gem HCl alone at E14 ($P < 0.01$), confirming the potential of the developed formulation.

4.3.4.3. Histopathological analysis. Histopathological evaluation of haematoxylin and eosin (H&E) stained sections was performed to assess tumour morphology changes in MDA-MB-231-CAM xenograft following treatment (Fig. 11.5). The control group exhibited densely packed tumour cells with pleomorphic, hyperchromatic nuclei and visible vascular structures (Fig. 11.5-A). Tumours treated with free Gem HCl showed reduced cellularity, nuclear condensation and fragmentation, and stromal alteration, with residual tumour tissue remaining evident (Fig. 11.5-B).

In comparison, representative sections from the HA-Gem HCl: APOBEC3B siRNA-NLC-treated group showed more pronounced morphological changes, including areas consistent with necrosis, reduced cellularity, nuclear fragmentation, and disrupted tissue architecture (Fig. 11.5-C). These findings suggest treatment-associated histological alterations; however, H&E staining alone cannot establish the mechanism of cell death or confirm antiangiogenic activity.

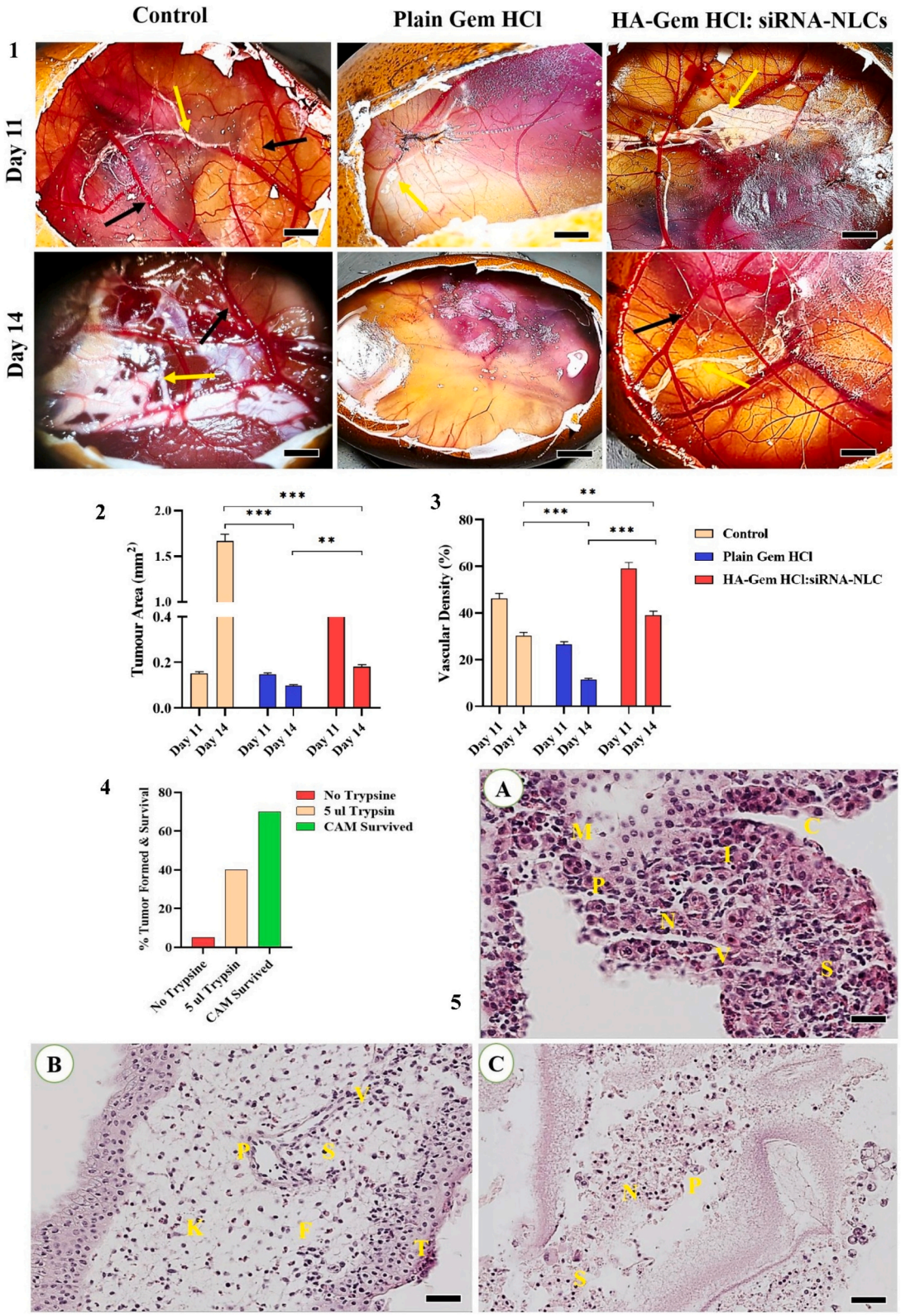

Fig. 11. Evaluation of MDA-MB-231 xenografts using the chick chorioallantoic membrane (CAM) model. (1) Representative macroscopic images of CAM tumours before (E11) and after (E14) treatment with DPBS (control), free Gem HCl or HA-Gem HCl: APOBEC3B siRNA-NLC (scale bars = 2 mm). Yellow arrows indicate tumour masses, and black arrows indicate blood vessels. Quantitative analysis: (2) Tumour area (mm^2) and (3) vascular density (% image area) in MDA-MB-231 xenograft on CAM at E11 and E14 across treatment groups. Data represent mean ± SEM ($n = 3$), $^{**}p < 0.01$, $^{***}p < 0.001$. (4) Percentage of successful tumour engraftment with and without trypsin pretreatment and overall embryo survival to E14. (3) Representative haematoxylin and eosin (H&E)-stained tumour sections (400× magnification; scale bars = 50 μm). (A) Control group showing densely packed tumour cells, including mitotic figures (M), (P) pleomorphic nuclei, (V) vascular structures, and (S) Stroma. (B) Free Gem HCl-treated group showing stromal alterations (S), reduced cellularity (F) and residual tumour cells (T). (C) HA-Gem HCl: APOBEC3B siRNA-NLCs treated group showing areas consistent with necrosis (N), nuclear condensation and fragmentation (P), and altered stromal architecture (S).

5. Discussion

5.1. Efficient APOBEC3B gene silencing and targeted siRNA delivery

APOBEC3B has emerged as an important therapeutic target in TNBC because its overexpression promotes genomic instability, tumour evolution and resistance to DNA-damaging therapies through continuous mutagenesis [14,35]. The selected siRNA (C) sequence effectively suppressed APOBEC3B expression without detectable nonspecific effects, confirming sequence-specific RNA interference. The magnitude of APOBEC3B suppression achieved here is expected to substantially attenuate APOBEC3B-driven mutagenesis, thereby reducing mutational heterogeneity and potentially sensitising tumour cells to Gem HCl, a chemotherapeutic whose efficacy is directly compromised by the APOBEC3B-mediated DNA damage tolerance mechanism [36]. Comparable APOBEC3B knockdown efficiencies that have been reported by Manikandan et al. revealed that APOBEC3B silencing restored cisplatin sensitivity in resistant cells, whereas APOBEC3B knockout significantly increased chemosensitivity [37], and Emily et al. demonstrated that APOBEC3B overexpression promotes tamoxifen resistance, and its inhibition may enhance the efficacy of targeted therapies [18]. However, these studies largely employed conventional transfection reagents rather than clinically translatable nanocarriers. In the present study, the encapsulation of APOBEC3 siRNA (C) within the NLC lipid matrix (EE% 68.29%) is expected to confer substantial protection against serum nuclease-mediated degradation, as the electrostatic interaction between the negatively charged siRNA phosphodiester backbone and the lipid surface physically restricts direct RNase accessibility to the siRNA substrate [38,39]. The preserved gene-silencing bioactivity of siRNA C)-NLCs (97.0% APOBEC3B Knockdown) is functionally equivalent to intact Lipofectamine-delivered free siRNA (C) (97.7%), providing strong functional evidence that siRNA retained full structural integrity throughout formulation and intracellular delivery, since nuclease-degraded siRNA is incapable of RISC loading or sequence-specific mRNA cleavage. These findings align with Senel B et al. and Mennati A et al., who confirmed siRNA structural integrity in a co-loaded NLC system by maintaining gene-silencing activity after cellular delivery [5,23]. Our results demonstrated that NLC encapsulation preserved RNAi activity while avoiding the cytotoxicity commonly associated with cationic lipid transfection reagents, supporting NLCs as a clinically translatable and nuclease-protective vehicle for APOBEC3B-targeted siRNA therapy in TNBC [23,40,41].

5.2. Formulation optimisation and physicochemical characteristics

The dominance of Labrasol as the principal determinant of entrapment efficiency and Tween 80 as the critical factor governing particle size, identified through BBD Optimisation, reflects the well-established physicochemical behaviour of lipid-based nanocarriers. Liquid lipid incorporation disrupts the ordered crystalline lattice of the solid lipid matrix, generating structural imperfections that enhance payload accommodation [42]. The micellar solubilization effect of excess Tween 80 on drug partitioning into the aqueous phase, observed here as a reduction in %EE at higher surfactant concentration, is consistent with the findings reported by Iqbal et al. [42] and Rao et al. [43]. The near-neutral zeta potential of uncoated NLCs is due to the presence of phosphatidylcholine, which acts as a co-emulsifier and stabilises the lipid-water interface, thereby minimising droplet coalescence during nanoparticle formation, whilst providing limited electrostatic stabilisation, which is compensated by steric stabilisation from the non-ionic surfactant [41,44]. The successful co-encapsulation of Gem HCl and APOBEC3B siRNA within the NLC matrix without compromising the physicochemical integrity of the formulation suggests minimal interference between the two cargoes during the encapsulation process. Both cargoes were efficiently incorporated; however, siRNA entrapment remained lower than that of Gem HCl. This difference is expected because Gem HCl partitions within the imperfect lipid matrix created by the mixed solid-lipid systems. In contrast, the large hydrophilic and negatively charged siRNA molecules are predominantly adsorbed near the particle surface through electrostatic interaction rather than being deeply embedded within the lipid core [45–47]. This spatial segregation prevents direct molecular contact and competitive displacement between Gem HCl and APOBEC3B siRNA during the formulation process, as evidenced by maintained high encapsulation efficiencies independently, and the stable PDI and zeta potential indicate co-loading did not disrupt colloidal integrity. Similar reduction in siRNA encapsulation has been reported in lipid nanoparticles developed by Huang et al. and Zhai et al., highlighting the inherent challenge of incorporating macromolecular nucleic acid into lipid matrices compared with small molecule drugs [48,49]. Following HA coating, the marked shift in zeta potential confirmed successful surface functionalization through electrostatic adsorption, consistent with the HA-coated nanocarrier system reported previously [31,50]. The increase in hydrodynamic diameter with HA concentration reflects progressive polymer shell formation and a possible bridging effect, as documented for similar HA-coated lipid nanoparticles [50,51]. Although HA coating enhanced CD44-mediated uptake [52] it gradually increased the particle size while remaining within the acceptable range; however, Motamedifer et al. reported that the larger particle size may reduce diffusion through the dense extracellular matrix of solid tumours [53]. Future studies should optimise HA density to balance receptor targeting with deep tumour penetration. FTIR analysis confirmed successful drug-HA incorporation through non-covalent interaction without chemical degradation, providing structural evidence of formulation integrity.

5.3. Co-delivery, sustained release and intracellular targeting

The sustained release profile and non-Fickian release behaviour indicate that both the lipid matrix and HA shell contributed to prolonged release of Gem HCl and APOBEC3B siRNA, which may improve therapeutic exposure while minimising premature drug leakage. The differential release profiles of both cargoes from the HA-NLC matrix reflect mechanistically distinct and independent release processes, where Gem HCl undergoes diffusion-driven release from the lipid matrix and siRNA release through surface desorption, confirming that co-encapsulation does not result in competitive interfering release kinetics. However, an excessively slow-release profile may delay the initial therapeutic onset, particularly in rapidly proliferating tumours requiring immediate cytotoxic concentration. Therefore, optimisation of HA and lipid composition will be important to balance early drug availability with prolonged exposure. In several HA-based nanocarriers, drug release is engineered to occur intracellularly rather than extracellularly to enhance tumour-selective cytotoxicity [54]. For example, Song et al. reported that redox-responsive HA-PTX conjugates and HA-based micelles undergo CD44-mediated endocytosis, followed by efficient PTX release in a glutathione-rich reductive cytosolic environment [55]. The chemotherapy resistance in TNBC was studied by [56,57] in which siRNA nanocarrier co-delivered with chemotherapy demonstrated true re-sensitisation of resistant TNBC cells beyond simple combination effects. CLSM confirmation of cytoplasmic and perinuclear localisation with significantly higher uptake in HA-coated *versus* uncoated NLCs is consistent with the CD44 overexpression profile of MDA-MB-231 cells, suggesting efficient cellular uptake and intracellular localisation rather than nonspecific surface adsorption and is justified by reported data on the receptor-mediated uptake pattern for folate-functionalized NLCs in the MDA-MB-231 cells [58,59].

5.4. Apoptosis, cell cycle disruption and anti-migratory activity

Annexin V-FITC/PI flow cytometry and cell cycle analysis revealed that all active treatment groups induced measurable apoptosis and cell cycle perturbation in MDA-MB-231 cells relative to the untreated

control and blank NLC group, with the latter confirming the biocompatibility of the unloaded carrier system. Free Gem HCl produced the highest acute G2/M accumulation and total apoptotic fraction at the 24-h observation point, attributable to its immediate bioavailability and rapid, burst cytotoxic action. The therapeutic superiority of HA-Gem HCl: APOBEC3B siRNA-NLC over free drug cannot be assessed solely based on single time-point acute readouts, for three interconnected mechanistic reasons.

First, the HA macromolecular surface coating introduces an additional diffusion barrier over the NLC lipid matrix, retarding Gem HCl and siRNA release relative to both uncoated NLCs and free drug, producing a controlled, sustained intracellular drug exposure profile that distributes cytotoxic activity progressively beyond the 24-h window, meaning the apoptotic and cell cycle responses measured at this single time point represent an underestimate of the formulation's full therapeutic potential. Second, HA-Gem HCl: APOBEC3B siRNA NLCs simultaneously silenced APOBEC3B mRNA, suppressing the DNA damage tolerance pathway that enables tumour cells to bypass genotoxic stress, a mechanistic contribution absent in the free Gem HCl group. Third, unlike free Gem HCl, which acts non-selectively, HA-NLC-mediated cytotoxicity is tumour-selective through CD44 receptor-mediated internalisation.

The mechanistic distinctiveness of the HA-NLC combination response is further evidenced by the substantially reduced S-phase population and elevated Sub-G1 fraction observed with HA-Gem HCl: APOBEC3B siRNA-NLCs, indicating active suppression of DNA synthesis and progressive apoptotic commitment, consistent with sustained rather than acute replication interference [17,60,61].

Importantly, the superior apoptotic response of Gem HCl: APOBEC3B siRNA-NLCs (50.2%) over Gem HCl-NLCs directly confirms the additive contribution of APOBEC3B gene silencing to chemosensitisation, whilst the enhanced activity of HA-Gem HCl: APOBEC3B siRNA NLCs relative to the non-targeted counterpart confirms further benefits of CD44-mediated active targeting. Collectively, the data established that the potential of HA-NLC formulation was not fully captured at 24 h, and is expected to produce progressively superior antitumour activity at extended time points.

Notably, Chen et al. demonstrated that gemcitabine induces autophagy in MDA-MB-231 cells, which acts cytoprotectively to inhibit apoptosis, a resistance mechanism that APOBEC3B suppression may partially counteract by reducing the genomic plasticity required to sustain the autophagic survival response [62]. Similar enhancement of apoptosis after siRNA-mediated chemosensitisation has been reported, where co-delivery systems induced significantly greater Annexin V positivity than free chemotherapy. Chen et al. [63] reported significantly higher apoptosis in a co-delivery system of doxorubicin and BCL2 siRNA compared to doxorubicin alone. Norouzi et al. [64] revealed that co-delivering NF-kB siRNA and gemcitabine achieves higher apoptosis compared to free gemcitabine in AsPC-1 cells. Likewise, Yan et al. [65] confirmed effective synergistic cytotoxicity through dual siRNA and chemotherapy delivery in cancer cells [66]. Regarding the potential interference between both cargoes on biological activity, both agents work through different mechanisms: Gem HCl blocks DNA synthesis while APOBEC3B siRNA reduces genomic instability at the gene level, indicating they are unlikely to interfere with each other's biological function. This is further supported by the fact that siRNA is located on the NLCs surface whilst Gem HCl is encapsulated within the lipid core, keeping both agents physically separated and preserving their individual activity after cellular uptake. The superior cytotoxicity, enhanced apoptosis and significant G2/M arrest and APOBEC3B gene silencing achieved simultaneously by HA-Gem HCl: APOBEC3B siRNA-NLCs collectively confirm pharmacodynamic complementarity and establish this formulation as a mechanistically progressive therapeutic strategy over free gemcitabine or any single-agent approach in MDA-MB-231 TNBC cells.

5.5. CAM xenograft validation and histopathological evidence

The CAM model provides a useful platform for preliminary evaluation of anti-tumour response [67,68] and is used as a fast, high-fidelity, aligned bridge between cell culture and rodent studies, generating efficacy data more relevant to humans, reducing both cost and animal use whilst generating preliminary *in vivo* evidence and strengthening the case for later *in vivo* validation of tumour growth inhibition and anti-angiogenic activity in a vascularised tumour microenvironment.

Previous studies have demonstrated its application in investigating tumour growth and angiogenesis in breast cancer xenografts [69] [70], as well as evaluating lipid-based nanocarrier formulation [71,72]. In the present study, macroscopic observations suggested differences in tumour appearance between the control, free Gem HCl and HA-Gem HCl: APOBEC3B siRNA-NLC-treated groups. Histopathological examination using H&E staining revealed treatment-associated morphological changes, including areas consistent with necrosis, reduced cellularity, nuclear fragmentation and disrupted tissue architecture in the combination-treated sections. Although these findings suggest a potential treatment response, the absence of quantitative tumour measurements and additional treatment controls prevents definitive conclusions regarding antitumour efficacy or the individual contributions of the formulation components. Furthermore, H&E staining alone cannot establish antiangiogenic activity without vascular assessment. Therefore, these preliminary findings warrant further quantitative and mechanistic investigations.

6. Limitations and future perspectives

Despite the encouraging findings, several limitations should be acknowledged. First, the biological evaluation was limited to the MDA-MB-231 TNBC cell line, and validation using additional TNBC models would improve the generalisability of the findings. Second, although the CAM model provides a rapid and cost-effective platform for preliminary tumour assessment, the absence of additional treatment controls and quantitative tumour measurements limits the interpretation of antitumour efficacy and the individual contributions of the formulation components. Furthermore, H&E staining alone cannot confirm antiangiogenic activity without quantitative vascular assessment and endothelial-specific markers. Third, the CAM model lacks a fully developed adaptive immune system and cannot fully reproduce the mammalian tumour microenvironment. Systemic pharmacokinetics, biodistribution, long-term toxicity and immune responses were not investigated. Future studies should therefore incorporate additional treatment controls, quantitative tumour and vascular analyses, and validation in more advanced tumour models. Long-term formulation stability, manufacturing reproducibility and regulatory considerations also require further investigations.

7. Conclusion

The present study successfully developed and optimised HA-coated NLCs for targeted co-delivery of Gem HCl and APOBEC3B siRNA to TNBC cells. The selected APOBEC3B siRNA (C) demonstrated substantial mRNA knockdown, which was maintained following NLC encapsulation. The optimised formulation exhibited favourable physicochemical characteristics, enhanced cellular uptake and promising *in vitro* cytotoxicity activity. In the CAM xenograft model, macroscopic and H&E histopathological observations revealed treatment-associated morphological changes, including areas consistent with necrosis, reduced tumour cellularity and disrupted tissue architecture. Although these preliminary findings are encouraging, further quantitative and mechanistic investigations are required to establish the individual contributions of the formulation components and confirm therapeutic efficacy. Overall, the developed HA-coated NLC system represents a promising platform for further investigation of combined drug and siRNA delivery

in TNBC.

CRediT authorship contribution statement

Sheikh Shahnawaz Quadir: Writing – review & editing, Writing – original draft, Methodology, Investigation. **Lauren Tonge:** Software. **Kehinde Ross:** Resources, Formal analysis. **Rasha Swadi:** Resources, Formal analysis. **Garima Joshi:** Supervision. **Imran Saleem:** Visualization, Supervision, Conceptualization.

Declaration of competing interests

The authors declare that they have no known competing financial interests or personal relationships that could have appeared to influence the work reported in this paper.

Acknowledgement

The authors gratefully acknowledge the financial support provided by the Commonwealth Scholarship Commission (CSC), United Kingdom, through the Commonwealth Split-Site Scholarship Programme (Ref. no: INCN-2024-263). This support enabled Mr. Sheikh Shahnawaz Sheikh Israil Quadir to undertake research in Nanomedicines at the School of Pharmacy and Biomolecular Sciences, Liverpool John Moores University (LJMU), United Kingdom. The authors sincerely thank Prof. Imran Saleem, LJMU, for his valuable guidance and mentorship as the UK host supervisor. The authors also express their gratitude to Dr. Garima Joshi, Department of Pharmaceutical Sciences, Mohanlal Sukhadia University, Udaipur, India, for her continuous support and supervision as the home institution mentor. Their invaluable contributions and collaborative efforts were instrumental in the successful completion of this research.

Data availability

Data will be made available on request.

References

[1] M. Attar, F.T. Shamsabadi, A. Soltani, M.T. Joghataei, S.R. khandoozi, S. Teimourian, M. Shahbazi, V. Erfani-Moghadam, Co-delivery of shRNA-linc-ROR and paclitaxel drug by cationic nanostructured lipid carrier (NLC) for breast cancer therapy: in vitro and in vivo, J. Drug Delivery Sci. Technol. (2025) 107941, https://doi.org/10.1016/j.jddst.2025.107941.

[2] M. Ashrafizadeh, A. Zarrabi, A. Bigham, A. Taheriazam, Y. Saghari, S. Mirzaei, M. Hashemi, K. Hushmandi, H. Karimi-Maleh, E. Nazarzadeh Zare, E. Sharifi, Y. N. Ertas, N. Rabiee, G. Sethi, M. Shen, (Nano)platforms in breast cancer therapy: drug/gene delivery, advanced nanocarriers and immunotherapy, Med. Res. Rev. 43 (2023) 2115–2176, https://doi.org/10.1002/med.21971.

[3] J. Yu, Q. Mu, M. Fung, X. Xu, L. Zhu, R.J.Y. Ho, Challenges and opportunities in metastatic breast cancer treatments: nano-drug combinations delivered preferentially to metastatic cells may enhance therapeutic response, Pharmacol. Ther. 236 (2022) 108108, https://doi.org/10.1016/J.PHARMTHERA.2022.108108.

[4] E. Masoumi, S. Tahaghoghi-Hajghorbani, L. Jafarzadeh, M.J. Sanaei, A. Pourbagheri-Sigaroodi, D. Bashash, The application of immune checkpoint blockade in breast cancer and the emerging role of nanoparticle, J. Control. Release 340 (2021) 168–187, https://doi.org/10.1016/J.JCONREL.2021.10.018.

[5] A. Mennati, K. Rostamizadeh, H.K. Manjili, M. Fathi, H. Danafar, Co-delivery of siRNA and lycopene encapsulated hybrid lipid nanoparticles for dual silencing of insulin-like growth factor 1 receptor in MCF-7 breast cancer cell line, Int. J. Biol. Macromol. 200 (2022) 335–349, https://doi.org/10.1016/J.IJBIOMAC.2021.12.197.

[6] V. Jadhav, A. Vaishnaw, K. Fitzgerald, M.A. Maier, RNA interference in the era of nucleic acid therapeutics, Nat. Biotechnol. 42 (2024) 394–405, https://doi.org/10.1038/s41587-023-02105-y.

[7] E. Shcherbinina, M. Fong, A. Biscans, A.A. Sarshad, Argonaute and small RNAs in the nucleus: mediators of gene silencing and activation, Mol. Ther. Nucleic Acids 37 (2026), https://doi.org/10.1016/j.omtn.2026.102938.

[8] K. Ui-Tei, Progress in siRNA nucleic acid therapeutics and challenges in their application to cancer treatment, Jpn. J. Clin. Oncol. 2026 (n.d.) 1–10. doi:https://doi.org/10.1093/jjco/hyag099/8724548.

[9] A. Talebi, A. Khorrami, F. Oruji, S. Shabani, S. Hajazimian, H. Nasiri, S. Khansalar, A. Isazadeh, M. Akbari, Small interfering RNA (siRNA)-based targeting breast cancer therapy, Discov. Oncol. (2026), https://doi.org/10.1007/s12672-026-04885-6.

[10] M. Banerjee, V.D. Rajeswari, Critical review on the different roles of exosomes in TNBC and exosomal-mediated delivery of microRNA/siRNA/lncRNA and drug targeting signalling pathways in triple-negative breast cancer, Molecules 28 (2023), https://doi.org/10.3390/molecules28041802.

[11] N. Laxane, K.S. Yadav, Recent advances in nanocarrier systems for the co-delivery of siRNA and chemotherapeutic drug for breast cancer therapy, Cancer Investig. 43 (2025) 694–713, https://doi.org/10.1080/07357907.2025.2559088.

[12] M. Petljak, A. Dananberg, K. Chu, E.N. Bergstrom, J. Striepen, P. von Morgen, Y. Chen, H. Shah, J.E. Sale, L.B. Alexandrov, M.R. Stratton, J. Maciejowski, Mechanisms of APOBEC3 mutagenesis in human cancer cells, Nature 607 (2022) 799–807, https://doi.org/10.1038/s41586-022-04972-y.

[13] K. Shi, M.A. Carpenter, S. Banerjee, N.M. Shaban, K. Kurahashi, D.J. Salamango, J. L. McCann, G.J. Starrett, J.V. Duffy, Ö. Demir, R.E. Amaro, D.A. Harki, R.S. Harris, H. Aihara, Structural basis for targeted DNA cytosine deamination and mutagenesis by APOBEC3A and APOBEC3B, Nat. Struct. Mol. Biol. 24 (2017) 131–139, https://doi.org/10.1038/nsmb.3344.

[14] F. Zhou, W. Chen, L. Ruan, The role of APOBEC3B in cancer: mechanisms, clinical challenges, and therapeutic opportunities, Hum. Mutat. 2026 (2026), https://doi.org/10.1155/humu/4838966.

[15] M.B. Burns, L. Lackey, M.A. Carpenter, A. Rathore, A.M. Land, B. Leonard, E. W. Refsland, D. Kotandeniya, N. Tretyakova, J.B. Nikas, D. Yee, N.A. Temiz, D. E. Donohue, R.M. Mcdougle, W.L. Brown, E.K. Law, R.S. Harris, APOBEC3B is an enzymatic source of mutation in breast cancer, Nature 494 (2013) 366–370, https://doi.org/10.1038/nature11881.

[16] S.A. Roberts, M.S. Lawrence, L.J. Klimczak, S.A. Grimm, D. Fargo, P. Stojanov, A. Kiezun, G.V. Kryukov, S.L. Carter, G. Saksena, S. Harris, R.R. Shah, M. A. Resnick, G. Getz, D.A. Gordenin, An APOBEC cytidine deaminase mutagenesis pattern is widespread in human cancers, Nat. Genet. 45 (2013) 970–976, https://doi.org/10.1038/ng.2702.

[17] M.B. Burns, N.A. Temiz, R.S. Harris, Evidence for APOBEC3B mutagenesis in multiple human cancers, Nat. Genet. 45 (2013) 977–983, https://doi.org/10.1038/ng.2701.

[18] E.K. Law, A.M. Sieuwerts, K. Lapara, B. Leonard, G.J. Starrett, A.M. Molan, N.A. Temiz, R.I. Vogel, M.E. Meijer-Van Gelder, F.C.G.J. Sweep, P.N. Span, J.A. Foekens, J.W.M. Martens, D. Yee, R.S. Harris, H E A L T H A N D M E D I C I N E The DNA Cytosine Deaminase APOBEC3B Promotes Tamoxifen Resistance in ER-positive Breast Cancer, n.d. https://www.science.org.

[19] A. Gupta, A. Gazzo, P. Selenica, A. Safonov, F. Pareja, E.M. da Silva, D.N. Brown, H. Shao, Y. Zhu, J. Patel, J. Blanco-Heredia, B. Stefanovska, M.A. Carpenter, Y. Chen, I. Vegas, X. Pei, D. Frosina, A.A. Jungbluth, M. Ladanyi, G. Curigliano, B. Weigelt, N. Riaz, S.N. Powell, P. Razavi, R.S. Harris, J.S. Reis-Filho, A. Marra, S. Chandarlapaty, APOBEC3 mutagenesis drives therapy resistance in breast cancer, Nat. Genet. 57 (2025) 1452–1462, https://doi.org/10.1038/s41588-025-02187-1.

[20] P.A. Roelofs, M.A.M. Timmermans, B. Stefanovska, M.A. den Boestert, A.W.M. van den Borne, H.E. Balcioglu, A.M. Trapman, R.S. Harris, J.W.M. Martens, P.N. Span, Aberrant APOBEC3B expression in breast cancer is linked to proliferation and cell cycle phase, Cells 12 (2023), https://doi.org/10.3390/cells12081185.

[21] O. Onguru, S. Yalcin, C. Rosemblit, P.J. Zhang, S. Kilic, U. Gunduz, APOBEC3B expression in drug resistant MCF-7 breast cancer cell lines, Biomed. Pharmacother. 79 (2016) 87–92, https://doi.org/10.1016/j.biopha.2016.02.004.

[22] A.M. Sieuwerts, W.A.M.E. Schrijver, S.U. Dalm, V. De Weerd, C.B. Moelans, N. Ter Hoeve, P.J. Van Diest, J.W.M. Martens, C.H.M. Van Deurzen, Progressive APOBEC3B mRNA expression in distant breast cancer metastases, PLoS One 12 (2017), https://doi.org/10.1371/journal.pone.0171343.

[23] B. Şenel, E. Başaran, E. Akyıl, U.M. Güven, G. Büyükköroğlu, Co-delivery of siRNA and docetaxel to cancer cells by NLC for therapy, ACS Omega 9 (2024) 11671–11685, https://doi.org/10.1021/acsomega.3c09098.

[24] P. Norouzi, M. Amini, R. Dinarvand, E. Arefian, E. Seyedjafari, F. Atyabi, Co-delivery of gemcitabine prodrug along with anti NF-κB siRNA by tri-layer micelles can increase cytotoxicity, uptake and accumulation of the system in the cancers, Mater. Sci. Eng. C 116 (2020), https://doi.org/10.1016/j.msec.2020.111161.

[25] X. Zhao, F. Li, Y. Li, H. Wang, H. Ren, J. Chen, G. Nie, J. Hao, Co-delivery of HIF1α siRNA and gemcitabine via biocompatible lipid-polymer hybrid nanoparticles for effective treatment of pancreatic cancer, Biomaterials 46 (2015) 13–25, https://doi.org/10.1016/J.BIOMATERIALS.2014.12.028.

[26] H. Huang, Y. Mu, Y. Huang, B. Ji, Y. Wang, C.Y. Chen, Y. Chen, Z. Luo, S. Li, Z. Zhang, L. Wang, J.F. Conway, D. Yang, J. Wang, J. Sun, S. Li, Rational development of gemcitabine-based nanoplatform for targeting SERPINB9/Granzyme B axis to overcome chemo-immune-resistance, Nat. Commun. 16 (2025), https://doi.org/10.1038/s41467-025-59490-y.

[27] S. Ghosh, S. Dutta, A. Sarkar, M. Kundu, P.C. Sil, Targeted delivery of curcumin in breast cancer cells via hyaluronic acid modified mesoporous silica nanoparticle to enhance anticancer efficiency, Colloids Surf. B: Biointerfaces 197 (2021) 111404, https://doi.org/10.1016/J.COLSURFB.2020.111404.

[28] M. Tsuboi, A. Yamane, J. Horiguchi, T. Yokobori, R. Kawabata-Iwakawa, S. Yoshiyama, S. Rokudai, H. Odawara, H. Tokiniwa, T. Oyama, I. Takeyoshi, M. Nishiyama, APOBEC3B high expression status is associated with aggressive phenotype in Japanese breast cancers, Breast Cancer 23 (2016) 780–788, https://doi.org/10.1007/s12282-015-0641-8.

[29] S.S. Quadir, N. Panchal, A. Patel, D. Choudhary, K. Sawant, G. Joshi, Phosphatidylcholine bilayered paclitaxel-loaded NLCs to overcome intestinal barriers via dual endocytic pathways for enhanced efficacy in pancreatic cancer-in

silico to in vivo investigations, J. Drug Delivery Sci. Technol. 121 (2026), https://doi.org/10.1016/j.jddst.2026.108317.
[30] S.A. Bustin, V. Benes, J.A. Garson, J. Hellemans, J. Huggett, M. Kubista, R. Mueller, T. Nolan, M.W. Pfaffl, G.L. Shipley, J. Vandesompele, C.T. Wittwer, The MIQE guidelines: Minimum information for publication of quantitative real-time PCR experiments, Clin. Chem. 55 (2009) 611–622, https://doi.org/10.1373/clinchem.2008.112797.
[31] Y. Ma, J. Liu, X. Cui, J. Hou, F. Yu, J. Wang, X. Wang, C. Chen, L. Tong, Hyaluronic acid modified nanostructured lipid carrier for targeting delivery of kaempferol to NSCLC: preparation, optimization, characterization, and performance evaluation in vitro, Molecules 27 (2022), https://doi.org/10.3390/molecules27144553.
[32] G.M.L. Sys, L. Lapeire, N. Stevens, H. Favoreel, R. Forsyth, M. Bracke, O. De Wever, The in ovo CAM-assay as a xenograft model for sarcoma, J. Vis. Exp. (2013), https://doi.org/10.3791/50522.
[33] D. Ribatti, The chick embryo chorioallantoic membrane as an in vivo assay to study antiangiogenesis, Pharmaceuticals 3 (2010) 482–513, https://doi.org/10.3390/ph3030482.
[34] R. Swadi, G. Mather, B.L. Pizer, P.D. Losty, V. See, D. Moss, Optimising the chick chorioallantoic membrane xenograft model of neuroblastoma for drug delivery, BMC Cancer 18 (2018), https://doi.org/10.1186/s12885-017-3978-x.
[35] Z.W. Zhao, J.Q. Zhou, W. Bin Jia, Y. Xie, Y. Zhou, C.L. Ning, X.C. Cao, Y. Yu, X. Wang, Subtype-specific APOBEC enrichment links genomic instability to predict immunotherapy response in breast cancer subtypes, Int. J. Biol. Macromol. 356 (2026), https://doi.org/10.1016/j.ijbiomac.2026.151525.
[36] P.A. Roelofs, C.Y. Goh, B.H. Chua, M.C. Jarvis, T.A. Stewart, J.L. McCann, R. M. McDougle, M.A. Carpenter, J.W. Martens, P.N. Span, D. Kappei, R.S. Harris, Characterization of the mechanism by which the RB/E2F pathway controls expression of the cancer genomic DNA deaminase APOBEC3B, Elife 9 (2020), https://doi.org/10.7554/eLife.61287.
[37] M. Periyasamy, A.K. Singh, C. Gemma, R. Farzan, R.C. Allsopp, J.A. Shaw, S. Charmsaz, L.S. Young, P. Cunnea, R.C. Coombes, B. Győrffy, L. Buluwela, S. Ali, Induction of APOBEC3B expression by chemotherapy drugs is mediated by DNA-PK-directed activation of NF-κB, Oncogene 40 (2021) 1077–1090, https://doi.org/10.1038/s41388-020-01583-7.
[38] A. Gordillo-Galeano, C.E. Mora-Huertas, Solid lipid nanoparticles and nanostructured lipid carriers: a review emphasizing on particle structure and drug release, Eur. J. Pharm. Biopharm. 133 (2018) 285–308, https://doi.org/10.1016/J.EJPB.2018.10.017.
[39] J.A. Kulkarni, D. Witzigmann, S.B. Thomson, S. Chen, B.R. Leavitt, P.R. Cullis, R. van der Meel, The current landscape of nucleic acid therapeutics, Nat. Nanotechnol. 16 (2021) 630–643, https://doi.org/10.1038/s41565-021-00898-0.
[40] N.K. Garg, N. Tandel, S.K. Bhadada, R.K. Tyagi, Nanostructured lipid carrier–mediated transdermal delivery of aceclofenac hydrogel present an effective therapeutic approach for inflammatory diseases, Front. Pharmacol. 12 (2021), https://doi.org/10.3389/fphar.2021.713616.
[41] M. de C.V. Queiroz, L.A. Muehlmann, Characteristics and preparation of solid lipid nanoparticles and nanostructured lipid carriers, J. Nanotheranostics 5 (2024) 188–211, https://doi.org/10.3390/jnt5040012.
[42] W.A. Mahdi, S.I. Bukhari, S.S. Imam, S. Alshehri, A. Zafar, M. Yasir, Formulation and optimization of butenafine-loaded topical nano lipid carrier-based gel: characterization, irritation study, and anti-fungal activity, Pharmaceutics 13 (2021), https://doi.org/10.3390/pharmaceutics13071087.
[43] G.K. Rao, S. Jamadar, Tailoring Nanostructured Lipid Carriers for Efficient Delivery of Asenapine Maleate in Antipsychotic Treatment, 2024, https://doi.org/10.21203/rs.3.rs-4680275/v1.
[44] N.S. Kulkarni, N.S. Ranpise, D.S. Rathore, S.N. Dhole, Characterization of Self-microemulsifying Dosage Form: Special Emphasis on Zeta Potential Measurement. https://ssrn.com/abstract=3787937, 2019.
[45] J.A. Kulkarni, D. Witzigmann, S. Chen, P.R. Cullis, R. Van Der Meel, Lipid nanoparticle technology for clinical translation of siRNA therapeutics, Acc. Chem. Res. 52 (2019) 2435–2444, https://doi.org/10.1021/acs.accounts.9b00368.
[46] Y. Eygeris, M. Gupta, J. Kim, G. Sahay, Chemistry of lipid nanoparticles for RNA delivery, Acc. Chem. Res. 55 (2022) 2–12, https://doi.org/10.1021/acs.accounts.1c00544.
[47] A.Y. Antipina, A.A. Gurtovenko, Toward understanding liposome-based siRNA delivery vectors: atomic-scale insight into siRNA-lipid interactions, Langmuir 34 (2018) 8685–8693, https://doi.org/10.1021/acs.langmuir.8b01211.
[48] L. Huang, W. Guo, T. Zhao, Y. Feng, Y. Li, Q. An, C. Li, Y. Tian, H. Zhang, C. Zhou, Y. Sun, C. He, Z. Niu, H. Shen, B. Xiang, Microfluidic fabrication of lipid nanoparticles for co-delivery of siRNA and hydroxychloroquine: an engineered theranostic platform for enhanced breast cancer treatment, Chem. Eng. J. 506 (2025), https://doi.org/10.1016/j.cej.2025.160172.
[49] J. Zhai, A. Surian, T. Cote, W. Zhang, B.T. Dang, Y. Wang, Q. Chen, K. Hoshino, J. Lee, Y. Chen, Enhanced endosomal escape for nanoparticle-enabled co-delivery of doxorubicin and siRNA to overcome multidrug resistance, Mater. Today Adv. 30 (2026), https://doi.org/10.1016/j.mtadv.2026.100845.
[50] S. Song, H. Qi, J. Xu, P. Guo, F. Chen, F. Li, X. Yang, N. Sheng, Y. Wu, W. Pan, Hyaluronan-based nanocarriers with CD44-overexpressed cancer cell targeting, Pharm. Res. 31 (2014) 2988–3005, https://doi.org/10.1007/s11095-014-1393-4.
[51] P. Porbaha, R. Ansari, M.R. Kiafar, R. Bashiry, M.M. Khazaei, A. Dadbakhsh, A. Azadi, A comparative mathematical analysis of drug release from lipid-based nanoparticles, AAPS PharmSciTech 25 (2024), https://doi.org/10.1208/s12249-024-02922-7.
[52] S. Misra, P. Heldin, V.C. Hascall, N.K. Karamanos, S.S. Skandalis, R.R. Markwald, S. Ghatak, Hyaluronan-CD44 interactions as potential targets for cancer therapy, FEBS J. 278 (2011) 1429–1443, https://doi.org/10.1111/j.1742-4658.2011.08071.x.
[53] A. Motamedifar, H. Ghafouri, N. Alizadeh, Hyaluronic acid-coated magnetic solid lipid nanoparticles for cancer-targeted delivery of gemcitabine and imaging agent, Carbohydr. Polym. Technol. Appl. 11 (2025), https://doi.org/10.1016/j.carpta.2025.100946.
[54] A.M.A. Ballal, J.C. Nwabuife, W.S. Serumula, M.P. Sekhoacha, M. Faya, Application of hyaluronic acid in enhancing the efficacy and safety of paclitaxel nanoformulations for cancer treatment: a recent review, Bionanoscience 16 (2026), https://doi.org/10.1007/s12668-026-02653-y.
[55] Y. Song, H. Cai, T. Yin, M. Huo, P. Ma, J. Zhou, W. Lai, Paclitaxel-loaded redox-sensitive nanoparticles based on hyaluronic acid-vitamin E succinate conjugates for improved lung cancer treatment, Int. J. Nanomedicine 13 (2018) 1585–1600, https://doi.org/10.2147/IJN.S155383.
[56] P. Eivazy, F. Atyabi, F. Jadidi-Niaragh, L. Aghebati Maleki, A. Miahipour, J. Abdolalizadeh, M. Yousefi, The impact of the codelivery of drug-siRNA by trimethyl chitosan nanoparticles on the efficacy of chemotherapy for metastatic breast cancer cell line (MDA-MB-231), Artif. Cells Nanomed. Biotechnol. 45 (2017) 889–896, https://doi.org/10.1080/21691401.2016.1185727.
[57] A. Crintea, C.I. Bocșan, E.M. Jianu, A.S. Șovrea, C. Munteanu, M.P. Kubelac, A. M. Crăciun, C.N. Silaghi, Overcoming chemotherapy resistance in triple-negative breast cancer with nanocarrier-delivered siRNA therapeutics, J. Clin. Med. 15 (2026), https://doi.org/10.3390/jcm15062311.
[58] F.A. Soares, B. Salinas, S. Reis, C. Nunes, Hyaluronic acid-engineered milk extracellular vesicles to target triple negative breast cancer through CD44, Pharm. Biol. 63 (2025) 411–427, https://doi.org/10.1080/13880209.2025.2511807.
[59] A. Chaudhuri, D.N. Kumar, S.K. Srivastava, D. Kumar, U.K. Patil, A.S. Parmar, S. Singh, A.K. Agrawal, Combinatorial delivery of docetaxel- and erlotinib-loaded functionalized nanostructured lipid carriers for the treatment of triple-negative breast cancer using quality-by-design approach, Pharmaceutics 16 (2024), https://doi.org/10.3390/pharmaceutics16070926.
[60] E. Mini, S. Nobili, B. Caciagli, I. Landini, T. Mazzei, Cellular pharmacology of gemcitabine, Ann. Oncol. 17 (2006) v7–v12, https://doi.org/10.1093/ANNONC/MDJ941.
[61] T. Patel, A. Himaja, S. Biswas, B. Ghosh, Dual stimuli-responsive gemcitabine-conjugated alginate-chitosan nanoparticles for triple-negative breast cancer therapy: a smart approach, Bioconjug. Chem. 36 (2025) 2037–2053, https://doi.org/10.1021/acs.bioconjchem.5c00334.
[62] M. Chen, M. He, Y. Song, L. Chen, P. Xiao, X. Wan, F. Dai, P. Shen, The cytoprotective role of gemcitabine-induced autophagy associated with apoptosis inhibition in triple-negative MDA-MB-231 breast cancer cells, Int. J. Mol. Med. 34 (2014) 276–282, https://doi.org/10.3892/ijmm.2014.1772.
[63] A.M. Chen, M. Zhang, D. Wei, D. Stueber, O. Taratula, T. Minko, H. He, Co-delivery of Doxorubicin and Bcl-2 siRNA by mesoporous silica nanoparticles enhances the efficacy of chemotherapy in multidrug-resistant cancer cells, Small 5 (2009) 2673–2677, https://doi.org/10.1002/smll.200900621.
[64] P. Norouzi, M. Amini, R. Dinarvand, E. Arefian, E. Seyedjafari, F. Atyabi, Co-delivery of gemcitabine prodrug along with anti NF-κB siRNA by tri-layer micelles can increase cytotoxicity, uptake and accumulation of the system in the cancers, Mater. Sci. Eng. C 116 (2020) 111161, https://doi.org/10.1016/J.MSEC.2020.111161.
[65] T. Yan, S. Zhu, W. Hui, J. He, Z. Liu, J. Cheng, Chitosan based pH-responsive polymeric prodrug vector for enhanced tumor targeted co-delivery of doxorubicin and siRNA, Carbohydr. Polym. 250 (2020) 116781, https://doi.org/10.1016/J.CARBPOL.2020.116781.
[66] Y. Guo, H. Yu, X. Li, L. Liu, J. He, X. Wang, H. Zhang, Q. Zhang, J. Fu, R. Gu, H. Li, D. Xu, Q. Liu, S.D. Cang, APOBEC3B-driven mutations negatively regulated by P53 promote tumor progression and immunosuppressive microenvironment in prostate cancer, Mol. Cell. Biochem. (2025), https://doi.org/10.1007/s11010-025-05442-5.
[67] A. Thomas, J.S. Reis-Filho, C.E. Geyer, H.Y. Wen, Rare subtypes of triple negative breast cancer: current understanding and future directions, NPJ Breast Cancer 9 (2023), https://doi.org/10.1038/s41523-023-00554-x.
[68] D. Ribatti, The chick embryo chorioallantoic membrane (CAM) assay, Reprod. Toxicol. 70 (2017) 97–101, https://doi.org/10.1016/J.REPROTOX.2016.11.004.
[69] J. Chen, Z. Zhou, Y. Yao, J. Dai, D. Zhou, L. Wang, Q.Q. Zhang, Dipalmitoylphosphatidic acid inhibits breast cancer growth by suppressing angiogenesis via inhibition of the CUX1/FGF1/ HGF signalling pathway, J. Cell. Mol. Med. 22 (2018) 4760–4770, https://doi.org/10.1111/jcmm.13727.
[70] Y. Kang, S.C. Regmi, M.Y. Kim, S. Banskota, J. Gautam, D.H. Kim, J.A. Kim, Anti-angiogenic activity of macrolactin A and its succinyl derivative is mediated through inhibition of class i PI3K activity and its signaling, Arch. Pharm. Res. 38 (2015) 249–260, https://doi.org/10.1007/s12272-014-0535-x.
[71] P. Guo, J. Yang, D. Jia, M.A. Moses, D.T. Auguste, ICAM-1-targeted, Lcn2 siRNA-encapsulating liposomes are potent anti-angiogenic agents for triple negative breast cancer, Theranostics 6 (2016) 1–13, https://doi.org/10.7150/thno.12167.
[72] A. de Cristo Soares Alves, D. Rosane Dallemole, T. Medeiro Ciocheta, A. Ferreira Weber, S. da Silva Gündel, F. Visioli, F. Figueiró, S. Stanisçuaski Guterres, A. Raffin Pohlmann, Chicken embryo model for in vivo acute toxicological and antitumor efficacy evaluation of lipid nanocarrier containing doxorubicin, Int. J. Pharm. X 6 (2023), https://doi.org/10.1016/j.ijpx.2023.100193.